

# Heterogeneous Information-Bottleneck Coordination Graphs for Multi-Agent Reinforcement Learning

Wei Duan, Junyu Xuan, En Yu, Xiaoyu Yang, and Jie Lu  
 Australian Artificial Intelligence Institute (AAIL), University of Technology Sydney  
 {wei.duan, junyu.xuan, en.yu-1, jie.lu}@uts.edu.au, xiaoyu.yang-3@student.uts.edu.au

## Abstract

Coordination graphs are a central abstraction in cooperative multi-agent reinforcement learning (MARL), yet existing sparse-graph learners lack a *theoretically grounded* mechanism to decide which edges should exist and how much information each edge should carry. Current methods rely on heuristic criteria that offer no formal guarantee on the learned topology, and no principled way to allocate different communication capacities to structurally different agent relationships.

To address this, we propose **Heterogeneous Information-Bottleneck Coordination Graphs (HIBCG)**, which learns a group-aware sparse graph in which both edge existence and message capacity are theoretically justified. With the graph information bottleneck (GIB) serving as the underlying tool, HIBCG first constructs a group-aligned block-diagonal prior that provides a closed-form criterion for edge retention—determining which edges should exist and at what density per group block—and then controls per-agent feature bandwidth on the resulting topology, compressing messages to retain only task-relevant content. We prove that the group-aligned prior strictly tightens the variational bound on topology learning, that the objective decomposes per group block enabling differential edge control, and that capacity allocation follows a water-filling principle. Experiments on SMACv1, SMACv2, and MAgent Battle (up to 100 agents) demonstrate state-of-the-art coordination performance, with the largest gains on heterogeneous multi-role tasks and large-scale scenarios where existing methods fail to converge.

**Keywords.** Multi-agent reinforcement learning, coordination graph, graph learning, information bottleneck, graph neural network.

## 1 Introduction

Cooperative multi-agent reinforcement learning (MARL) relies on agents exchanging task-relevant information so that local decisions can be coordinated toward a shared team objective [1–4]. A *coordination graph* makes this communication selective by specifying which agent pairs exchange information at each step [5–7]. By keeping only informative links, sparse coordination graphs reduce noise aggregation, lower computation, and generalise better to unseen states [8–11]. The core open problem is therefore not *whether* to use a graph, but *how to learn* a graph whose topology is faithful to the underlying coordination structure of the task. Existing graph learners answer this question with *homogeneous* criteria—fixed thresholds [10], top- $k$  selection [9], variance payoffs [8], attention scores [12, 13], or dynamic factor-graph generation policies [14]—that treat every link with the same rule.

Two limitations remain. **(1) Edge existence is not theoretically grounded:** current sparse-graph learners keep or remove edges using heuristic scores, so they cannot formally decide how dense intra-group and inter-group connections should be when agents form functional sub-teams. **(2) Communication capacity is not structurally controlled:** even after a topology is learned, existing methods lack a principled way to allocate different message bandwidths to different agent relationships. A principled framework should therefore jointly learn the graph topology and control the feature bandwidth carried on that graph.

To address both limitations, we propose **Heterogeneous Information-Bottleneck Coordination Graphs (HIBCG)**, built on top of our earlier Group-Aware Coordination Graph (GACG) [10]. HIBCG frames MARL coordination as a *heterogeneous graph-learning problem*: jointly learning a per-layer topology

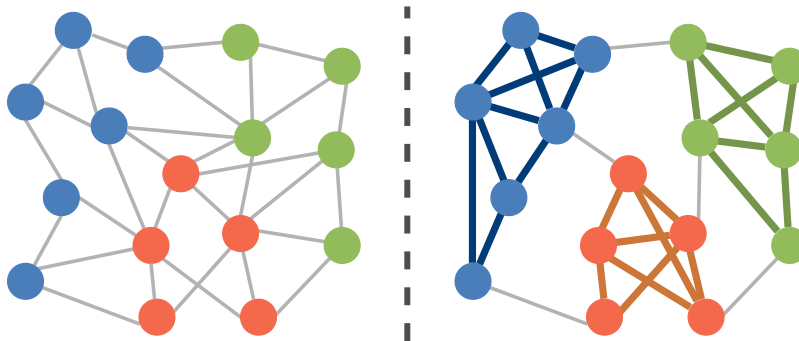


Figure 1: **Arbitrary vs. heterogeneous sparse coordination graphs.** Homogeneous sparsification (left) applies one criterion to all edges, producing sparse but structurally arbitrary links. HIBCG (right) learns a group-aligned sparse graph with dense intra-group connections and selective inter-group links. The pattern emerges from the group-aligned prior in Section 4, which gives different retention costs to different edge blocks.

that is sparse *in the right places* and a per-agent feature representation whose bandwidth is matched to that topology (Figure 1). Using the graph information bottleneck (GIB) as a *tool*—not as an end in itself—HIBCG couples two controls. **Topology learning** uses a group-aligned block-diagonal prior to provide a closed-form criterion for edge retention, making intra-group edges cheap to keep while requiring cross-group edges to justify their information cost. **Message control** then regulates the per-agent feature bandwidth on the learned topology, compressing messages so that the surviving communication channels carry task-relevant content. Together, these two controls learn not only which edges should exist, but also how much information should flow through the resulting graph.

### Contributions.

1. **A new method for heterogeneous coordination-graph learning.** HIBCG is, to our knowledge, the first method that jointly learns *which edges should exist* (with group-aware density control per block) and *how much information each edge carries* (with per-agent bandwidth allocation), using closed-form, per-layer Gaussian KL penalties built on a group-aligned block-diagonal prior.
2. **Theoretical guarantees via the GIB chain rule.** Five propositions establish formal properties of the learned graph: the joint objective decomposes into topology and feature paths (Prop. 4.1); the group-aligned prior *provably* tightens the variational bound with improvement growing with group-structure quality (Prop. 4.2); the topology term separates additively across group blocks (Prop. 4.3); the standard TD loss already maximises the relevance term (Prop. 4.4); and per-channel capacity follows a water-filling principle (Prop. 4.5).
3. **Broad empirical validation.** HIBCG adds only 3.8% wall-clock overhead. Experiments on SMACv1, SMACv2, and MAgent Battle (up to 100 agents) show state-of-the-art performance and scalability, with pronounced gains on heterogeneous multi-role tasks. Ablations confirm that the group-aligned prior—rather than the bottleneck per se—is the active ingredient.

The remainder of this paper is organised as follows. Section 2 reviews related work. Section 3 presents preliminaries. Section 4 develops the HIBCG framework following the three-stage architecture in Figure 2. Section 5 reports experiments. Section 7 concludes. All proofs and additional analyses are provided in the Appendix.

## 2 Related Work

### 2.1 Graph Learning for MARL

Graph neural networks (GNNs) [15–19] provide a natural substrate for MARL coordination, where agents are nodes and edges define information flow. Early graph-based MARL methods such as DGN [20], NerveNet [21], DCG [22], and DICG [12] showed that graph message passing can improve credit assignment and coordination. Later work focuses on learning more scalable or adaptive topologies: attention-based routing [13,23,24], sparse coordination graphs [8,9,25–27], recurrent graph message passing for generalisation [28], hand-designed scalable topologies [29,30], and dynamic factor-graph generation [14].

These methods improve *how* a graph is parameterised or updated, but edge existence is usually determined by homogeneous scores such as attention weights, thresholds, variance payoffs, or learned generation policies. They do not provide a theoretical criterion for deciding whether a particular edge should exist under different structural relationships. Role- and group-aware MARL methods, including ROMA [31], VAST [32], REFIL [33], SOG [34], GoMARL [35], and our earlier GACG [10], recognise that agents may form functional sub-teams. However, they still decide topology without a principled compression cost tied to each group block.

### 2.2 Communication-Efficient MARL

Communication is a second major axis of cooperative MARL. Classic differentiable communication methods [5,23,26] and scheduling or pruning methods [36–38] reduce when or with whom agents communicate, while information-theoretic methods such as NDQ [39], MASIA [40], and MAGI [41] encourage compact or robust messages. The information bottleneck principle [42–45] provides a natural language for this goal, and our earlier BVME [46] applies variational message compression on top of GACG’s sparse graph. However, these methods apply a global or topology-agnostic regulariser and do not couple message capacity with edge existence across structurally different group blocks. HIBCG makes this coupling explicit via per-block topology learning and per-agent message control. Advances in value decomposition [47], exploration [48,49], partial observability [6,7,11], policy optimisation [50], and non-stationary representation learning under concept drift [51–54] are complementary to our focus.

## 3 Preliminaries

### 3.1 Cooperative Dec-POMDPs

We consider cooperative multi-agent tasks modeled as a Decentralized Partially Observable Markov Decision Process (Dec-POMDP) [55] with tuple  $\langle \mathcal{A}, \mathcal{S}, \{\mathcal{U}_i\}_{i=1}^n, P, \{\mathcal{O}_i\}_{i=1}^n, \{\pi_i\}_{i=1}^n, R, \gamma \rangle$ . At time  $t$ , each agent  $i \in \mathcal{A}$  receives  $o_i^t \in \mathcal{O}_i$  and selects  $u_i^t \in \mathcal{U}_i$  via a local policy  $\pi_i(u_i^t | \tau_i^t)$  where  $\tau_i^t = (o_i^0, u_i^0, \dots, o_i^t)$ . The joint action  $\mathbf{u}^t = (u_1^t, \dots, u_n^t)$  yields the next state via  $P(s^{t+1} | s^t, \mathbf{u}^t)$  and a shared reward  $R(s^t, \mathbf{u}^t)$ . Over an episode of length  $T$  with discount  $\gamma \in [0, 1)$ , the goal is to maximize the discounted return; equivalently, learn a joint action-value  $Q_{\text{tot}}(s, \mathbf{u}) = \mathbb{E}[\sum_{t=0}^T \gamma^t R(s^t, \mathbf{u}^t) | s^0 = s, \mathbf{u}^0 = \mathbf{u}]$ , typically factored from per-agent utilities via monotonic mixing [56].

### 3.2 Group-Aware Coordination Graphs (GACG)

GACG learns a *Gaussian* distribution over all  $n^2$  candidate edges,

$$\text{vec}(\mathcal{E}^t) \sim \mathcal{N}(\boldsymbol{\mu}^t, \widehat{\mathbf{M}}^t), \quad (1)$$

with  $\boldsymbol{\mu}^t \in \mathbb{R}^{n^2}$  and  $\widehat{\mathbf{M}}^t \in \mathbb{R}^{n^2 \times n^2}$ . **Means** encode agent-pair importance: embeddings  $\hat{o}_i^t = f_{oe}(o_i^t)$  are scored as  $\mu_{ij}^t = f_{ap}(\hat{o}_i^t, \hat{o}_j^t)$  and vectorized into  $\boldsymbol{\mu}^t = \text{vec}([\mu_{ij}^t]_{i,j})$ . **Covariances** encode group-level dependence: groups  $\mathcal{G}^t = f_g(\mathcal{O}^{t-k:t})$  induce a block mask  $M_{ij}^t = \mathbb{I}[a_i, a_j \text{ in same group}]$  and  $\widehat{\mathbf{M}}^t = \text{vec}(M^t)\text{vec}(M^t)^\top$ , so co-group edges share higher correlated strength. Further details are given in GACG [10]. GACG determines *which* agents coordinate, but provides no mechanism to control *how much* information flows through the resulting graph—precisely the gap HIBCG fills (§4).

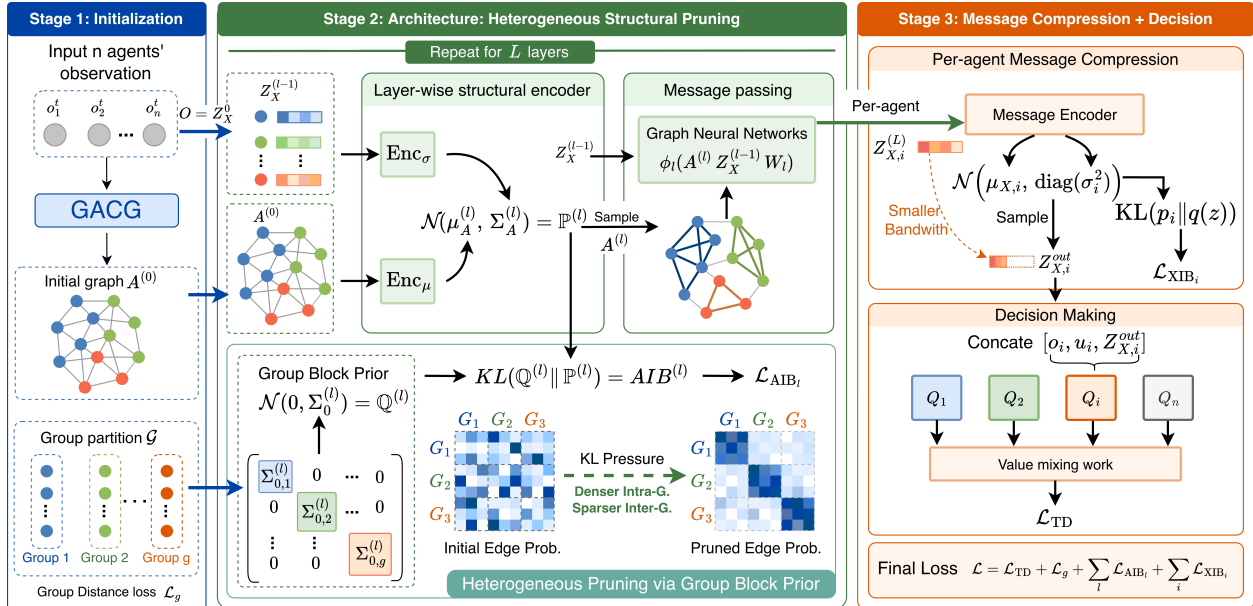


Figure 2: **HIBCG architecture overview.** **Stage 1 (Initialisation):** GACG produces the initial graph  $A^{(0)}$  and group partition  $\mathcal{G}$  from agent observations. **Stage 2 (Heterogeneous Structural Pruning):** At each GNN layer  $l$ , a layer-wise structural encoder maps  $(A^{(0)}, Z_X^{(l-1)})$  to Gaussian parameters  $\mathbb{P}^{(l)}$ ; the sampled adjacency  $A^{(l)}$  gates message passing. A group-aligned block-diagonal prior  $\mathbb{Q}^{(l)}$  applies asymmetric KL pressure: a larger  $\sigma_{0,\text{intra}}^2$  preserves dense intra-group edges while a smaller  $\sigma_{0,\text{inter}}^2$  aggressively prunes inter-group edges (bottom: initial vs. pruned edge probability). **Stage 3 (Message Compression + Decision):** After all  $L$  layers, a per-agent XIB encoder compresses the aggregated representation  $Z_{X,i}^{(L)}$  into a lower-bandwidth code  $Z_{X,i}^{\text{out}}$ , which is concatenated with local inputs for  $Q$ -value computation and value mixing. The final loss combines the TD error, the GACG group-distance loss, and the closed-form AIB and XIB KL penalties.

### 3.3 The Information Bottleneck Principle

The *information bottleneck* (IB) principle [42] provides a general framework for learning compressed representations that retain task-relevant information. Given input data  $\mathcal{D}$ , a task target  $Y$ , and a learned representation  $Z$ , the IB objective trades off *relevance* vs. *compression*:

$$\min_Z -I(Y; Z) + \beta I(\mathcal{D}; Z), \quad \beta > 0, \quad (2)$$

where  $I(\cdot; \cdot)$  denotes mutual information. The first term encourages  $Z$  to be predictive of  $Y$ ; the second penalizes the total information that  $Z$  retains about the raw input.

For graph-structured data  $\mathcal{D} = (A, X)$  processed by an  $L$ -layer GNN, the representation  $Z = Z_X^{(L)}$  is built through successive message-passing layers that produce intermediate latents for both graph structure  $\{Z_A^{(l)}\}$  and node features  $\{Z_X^{(l)}\}$ . Wu et al. [43] showed that the compression term  $I(\mathcal{D}; Z_X^{(L)})$  can be upper-bounded via layer-wise variational bounds, yielding practical, closed-form regularizers when the encoder distributions are Gaussian.

However, applying this principle to multi-agent coordination-graph learning raises several open questions that existing work does not address: *How should the total information flow on the graph be decomposed between topology learning and feature learning? How should the agents' group structure inform the structural prior? And how do the two learning paths interact?* We address all three in Section 4.

## 4 Method: HIBCG

We now develop HIBCG as a concrete heterogeneous coordination-graph learner for cooperative MARL. We first establish the theoretical foundation—five propositions that formalise the GIB-based objective for heterogeneous graph learning (§4.2)—and then show how these properties are instantiated as the three-stage architecture previewed in Figure 2: (Stage 1) GACG produces an initial group-aware graph  $A^{(0)}$  and partition  $\mathcal{G}$ ; (Stage 2) per-layer Gaussian structural encoders refine the topology via AIB; (Stage 3) per-agent XIB encoders compress messages for decentralised decision making. The full training procedure is in Appendix Algorithm 1.

### 4.1 Notation and Problem Setup

**Notation.** Let  $l \in \{1, \dots, L\}$  index message-passing layers and  $d_l$  the feature dimension at layer  $l$ . We write  $\mathcal{G}^t = \{g_1, \dots, g_m\}$  for the time-varying agent partition produced by GACG (§3.2); when the time superscript is clear from context we drop it. The data of a forward pass at time  $t$  is  $\mathcal{D} = (A, X)$ , where  $X = [x_1; \dots; x_n] \in \mathbb{R}^{n \times d_{\text{in}}}$  stacks per-agent input features (each  $x_i$  concatenates the local observation  $o_i$  with optional auxiliary inputs such as the last action and an agent identifier), and  $A$  is any explicit adjacency available at input time. Throughout,  $Z_X^{(l)} \in \mathbb{R}^{n \times d_l}$  denotes the per-agent feature latent at layer  $l$  and  $Z_A^{(l)}$  the structural latent (the layer- $l$  adjacency draw). For a group block  $g$  at layer  $l$ ,  $B_{l,g} \subseteq \{1, \dots, n\}^2$  collects the edges in that block and  $k_{l,g} = |B_{l,g}|$  is its size.

**Heterogeneous coordination-graph learning** We treat each forward pass as the outcome of a graph-learning procedure that produces, from  $\mathcal{D} = (A, X)$ , a sequence of pruned adjacencies  $\{Z_A^{(l)}\}_{l=1}^L$  and feature latents  $\{Z_X^{(l)}\}_{l=1}^L$ . A useful baseline is the *flat* regime in which all existing graph learners live:

**Definition 4.1** (Flat-IB coordination graph). *A flat-IB coordination graph is defined by a graph-learning loss of the form*

$$\mathcal{L} = \mathcal{L}_{\text{task}} + \beta \mathcal{R}(\theta), \quad \beta \geq 0, \quad (3)$$

where  $\mathcal{R}(\theta)$  is a single, global compression penalty (e.g., a KL on the entire GNN output) and  $\beta$  is a uniform trade-off weight applied identically to all agents, all edges, and all layers.

Definition 4.1 covers both explicit ( $\beta > 0$ , e.g. MAGI [41]) and implicit ( $\beta = 0$ , e.g. GACG [10], DCG [22]) flat-IB graph learners. In both cases the topology is **structurally indifferent**: within-group and cross-group edges are regularised identically, even though they typically play different coordination roles. We instead design a graph learner that respects this structural heterogeneity via (i) *group-aware priors* that assign different compression strengths to within- vs. cross-group blocks, (ii) *two coupled learning paths* (topology AIB + feature XIB, formally arising from the MI chain rule), and (iii) *per-layer regularisation* so each GNN layer carries its own compression diagnostic. The formal object is:

**Definition 4.2** (Heterogeneous IB coordination graph). *A heterogeneous IB coordination graph is defined by a graph-learning loss of the form*

$$\mathcal{L} = \mathcal{L}_{\text{task}} + \sum_{l,g} \lambda_A^{(l,g)} \mathcal{R}_A^{(l,g)}(\theta) + \sum_{l,i} \lambda_X^{(l,i)} \mathcal{R}_X^{(l,i)}(\theta), \quad (4)$$

where  $\mathcal{G} = \{g_1, \dots, g_m\}$  is a partition of agents into groups, inducing  $m^2$  edge blocks  $\mathcal{G}' \triangleq \{g_a \times g_b : g_a, g_b \in \mathcal{G}\}$  ( $a=b$  for within-group,  $a \neq b$  for cross-group);  $\mathcal{R}_A^{(l,g)}$  is a per-group, per-layer structural compression penalty on edge block  $g \in \mathcal{G}'$  at layer  $l$ ;  $\mathcal{R}_X^{(l,i)}$  is a per-agent, per-layer feature compression penalty; and  $\lambda_A^{(l,g)}, \lambda_X^{(l,i)} \geq 0$  are independent capacity weights. The structural prior is block-diagonal aligned with  $\mathcal{G}$ , so within-group and cross-group blocks can carry fundamentally different compression strengths. A flat-IB graph (Def. 4.1) is recovered by setting  $|\mathcal{G}| = 1$  and  $\lambda_A^{(l,g)} = \lambda_X^{(l,i)} = \beta$ .

Table 1: The three core contributions formalised as propositions. Each delivers a specific guarantee that defines HIBCG as a heterogeneous graph learner. Two supporting identities (Props. 4.1, 4.3) are standard tools, presented in §4.2 and detailed in the Appendix.

	Proposition	What it establishes	Role in HIBCG
4.2	Tighter bound via group-conditional priors	Group-aligned prior $\leq$ flat prior (in VUB), strict if $\mathbb{P}$ anisotropic	No-regret guarantee for topology learning; group structure never hurts
4.4	Relevance via $Q$ -value optimisation	$I(Y; Z_X^{(L)}) \geq H(Y) - f(\mathcal{L}_{\text{TD}})$	Standard TD loss already maximises the IB relevance term (no extra MI loss)
4.5	Optimal capacity allocation (water-filling)	KKT $\Rightarrow$ equal marginal utility across active channels	Principled heterogeneous allocation across topology and content channels

## 4.2 Theoretical Foundation: GIB-Based Heterogeneous Graph Learning

Treating the GNN forward pass as a stochastic graph learner that produces structural latents  $Z_A = \{Z_A^{(l)}\}_{l=1}^L$  and feature latents  $Z_X = \{Z_X^{(l)}\}_{l=1}^L$ , three properties are necessary for the heterogeneous design we want to build:

- (P1) **Structure/content decomposition**—a topology path (*which* edges to keep) cleanly separated from a content path (*what* flows on the surviving edges), so they can be independently regularised.
- (P2) **Group-structured prior with a no-regret guarantee**—the structural prior must admit per-block scales aligned with  $\mathcal{G}$  and never underperform a flat prior, so injecting group information adds upside without risk.
- (P3) **Closed-form, per-channel penalties**—both pruning and message control must reduce to differentiable per-block, per-agent KL terms that can carry independent weights  $\lambda_A^{(l,g)}, \lambda_X^{(l,i)}$ .

The graph information bottleneck (GIB) framework (2) supplies all three: GIB’s chain rule produces (P1) for free, a block-diagonal structural prior gives (P2) by Pinsker-type arguments, and Gaussian variational families realise (P3) as closed-form layer-wise KLs. The remainder of this subsection states the five propositions that formalise these properties; throughout, AIB and XIB are *tools for graph learning*, not the paper’s contribution. Propositions 4.1 and 4.3 record standard but necessary identities, while Propositions 4.2, 4.4, and 4.5 are the genuinely new claims summarised in Table 1. All proofs are in Sections E–J of the Appendix.

**(P1) Decomposition: AIB and XIB are the two halves of one chain rule.** The chain rule of mutual information, applied to  $(\mathcal{D}; Z_A, Z_X)$  and combined with a layer-wise variational bound, gives an *exact* split of the total information flow.

**Proposition 4.1** (Dual-Path Decomposition; standard). *Under the conditional independencies (CI-A):  $Z_A^{(l)} \perp (\mathcal{D}, Z_A^{(1:l-1)}) \mid (A^{(0)}, Z_X^{(l-1)})$  and (CI-X):  $Z_X^{(l)} \perp (\mathcal{D}, Z_X^{(1:l-2)}, Z_A^{(1:l-1)}) \mid (Z_X^{(l-1)}, Z_A^{(l)})$  induced by the message-passing recursion, the joint information flow factorises as*

$$I(\mathcal{D}; Z_A, Z_X) = \underbrace{I(\mathcal{D}; Z_A)}_{\text{AIB}} + \underbrace{I(\mathcal{D}; Z_X \mid Z_A)}_{\text{XIB}}, \quad (5)$$

and each term admits a per-layer variational upper bound:

$$I(\mathcal{D}; Z_A) \leq \sum_{l=1}^L \text{AIB}^{(l)}, \quad I(\mathcal{D}; Z_X \mid Z_A) \leq \sum_{l=1}^L \text{XIB}^{(l)}, \quad (6)$$

with  $\text{AIB}^{(l)} \triangleq \mathbb{E}[\text{KL}(\mathbb{P}(Z_A^{(l)} \mid A^{(0)}, Z_X^{(l-1)}) \parallel \mathbb{Q}(Z_A^{(l)}))]$  and  $\text{XIB}^{(l)}$  defined analogously for the message encoder  $\mathbb{P}(Z_X^{(l)} \mid Z_X^{(l-1)}, Z_A^{(l)})$ .

**Use in HIBCG.** Eq. (5) is the structural reason HIBCG splits into an AIB path and an XIB path: they are the two terms of a single decomposition, not two parallel regularizers. The conditional structure  $I(\mathcal{D}; Z_X | Z_A)$  further formalises the dependence in §4.1—message compression is defined *relative to* edge pruning, so tighter AIB pruning forces XIB to do more work on fewer surviving channels (§4.6).

**(P2) Bound tightening from a group-aligned prior.** Property (P1) leaves the prior  $\mathbb{Q}$  unspecified. The bounds in (6) are tight only insofar as  $\mathbb{Q}$  approximates the aggregate posterior  $\bar{\mathbb{P}} \triangleq \mathbb{E}_{\mathcal{D}}[\mathbb{P}(Z_A^{(l)} | \mathcal{D})]$ : the gap is exactly  $\text{KL}(\bar{\mathbb{P}} \| \mathbb{Q})$ . A flat prior  $\mathcal{N}(0, \sigma_0^2 I)$  ignores the agents’ group structure, so any block correlation in  $\bar{\mathbb{P}}$  is paid for as variational slack. We instead use a block-diagonal prior aligned with  $\mathcal{G}$ , which is provably no worse and strictly better whenever the groups are non-trivial.

**Proposition 4.2** (Tighter Bound via Group-Conditional Priors). *Let  $\mathbb{Q}_{\text{flat}}(Z_A^{(l)}) = \mathcal{N}(0, \sigma_0^2 I)$  be a flat isotropic prior and define the optimally matched group-aligned prior as*

$$\mathbb{Q}_{\text{group}}^*(Z_A^{(l)}) \triangleq \arg \min_{\mathbb{Q} \in \mathcal{Q}_{\text{blk}}} \text{KL}(\bar{\mathbb{P}}(Z_A^{(l)}) \| \mathbb{Q}), \quad (7)$$

where  $\mathcal{Q}_{\text{blk}} = \{\mathcal{N}(0, \text{blkdiag}(\Sigma_{0,g}^{(l)})_{g \in \mathcal{G}'}) : \Sigma_{0,g}^{(l)} \succ 0\}$  is the family of zero-mean block-diagonal Gaussian priors whose blocks are aligned with the group-block index set  $\mathcal{G}'$  (Def. 4.2), and  $\bar{\mathbb{P}}(Z_A^{(l)}) = \mathbb{E}_{\mathcal{D}}[\mathbb{P}(Z_A^{(l)} | \mathcal{D})]$  is the aggregate posterior. Then, unconditionally,

$$\mathbb{E}_{\mathcal{D}} \left[ \text{KL} \left( \mathbb{P}(Z_A^{(l)} | \mathcal{D}) \| \mathbb{Q}_{\text{group}}^* \right) \right] \leq \mathbb{E}_{\mathcal{D}} \left[ \text{KL} \left( \mathbb{P}(Z_A^{(l)} | \mathcal{D}) \| \mathbb{Q}_{\text{flat}} \right) \right]. \quad (8)$$

The gap equals  $\text{KL}(\bar{\mathbb{P}} \| \mathbb{Q}_{\text{flat}}) - \text{KL}(\bar{\mathbb{P}} \| \mathbb{Q}_{\text{group}}^*) \geq 0$  and is strict whenever  $\bar{\mathbb{P}}$  is not isotropic (i.e., different group blocks have different covariance scales).

*Proof.* See the Appendix for the proof. □

**Why this matters.** Because  $\mathbb{Q}_{\text{flat}} \in \mathcal{Q}_{\text{blk}}$ , the group-aligned prior is *never worse* than flat—a no-regret guarantee under *any* group partition the user supplies (Appendix F). The improvement is strict and proportional to how much the group blocks of  $\bar{\mathbb{P}}$  differ in scale: well-separated groups yield a large gap, while a homogeneous setting recovers the flat bound automatically. A worked  $n = 10$  example showing a  $> 75\%$  reduction of the bound gap is given in Appendix H; in our experiments the gap shrinks empirically by  $2.9\text{--}6.5\times$  across heterogeneous benchmarks (Table 3).

**(P3) Closed-form per-channel control.** Property (P2) restricts  $\mathbb{Q}$  to be block-diagonal. The next observation, an immediate consequence of KL additivity for product distributions, is what enables per-channel weights  $\lambda_A^{(l,g)}$ :

**Proposition 4.3** (Group-Aligned Block Decomposition; lemma). *If  $\mathbb{Q}(Z_A^{(l)}) = \mathcal{N}(0, \text{blkdiag}(\Sigma_{0,g}^{(l)})_{g \in \mathcal{G}'})$  and the encoder factorises over  $\mathcal{G}'$  as  $\mathbb{P}(Z_A^{(l)} | \mathcal{D}) = \prod_{g \in \mathcal{G}'} \mathbb{P}(Z_{A,g}^{(l)} | \mathcal{D})$ , then*

$$\text{AIB}^{(l)} = \sum_{g \in \mathcal{G}'} \text{AIB}^{(l,g)}, \quad \text{AIB}^{(l,g)} \triangleq \mathbb{E}_{\mathcal{D}} \left[ \text{KL} \left( \mathbb{P}(Z_{A,g}^{(l)} | \mathcal{D}) \| \mathbb{Q}(Z_{A,g}^{(l)}) \right) \right], \quad (9)$$

each summand being a closed-form Gaussian KL (Eq. (17)).

Eq. (9) is the technical reason we can attach independent capacity weights  $\lambda_A^{(l,g)}$  to each block. Setting  $\lambda_{\text{cross}} > \lambda_{\text{intra}}$  enforces sparse inter-team links while preserving dense intra-team connectivity—the heterogeneous edge pruning that defines HIBCG. (Proof: KL additivity, Appendix G.) Propositions 4.2–4.3 together turn the flat IB filter into a *structured force-field*: groups are now the natural unit of edge pruning.

**Relevance: TD loss is the right surrogate for IB relevance.** Property (P1) and (P2) together specify the *compression* side of the IB. The IB principle (2) also has a relevance term,  $-I(Y; Z_X^{(L)})$ , which is in general intractable. The next proposition shows this term is implicitly handled by the standard TD loss that any value-decomposition MARL pipeline is already minimising—so HIBCG does not require any separate mutual-information estimator.

**Proposition 4.4** (Relevance via Q-Value Optimization). *Let  $Y = (a_1^*, \dots, a_n^*)$  denote the optimal joint action and  $K = \prod_i |\mathcal{U}_i|$  the joint action-space size. Assume:*

- (A1) *QMIX-style monotonic value decomposition with greedy action selection  $a_i = \arg \max_{u_i} Q_i(\tau_i, u_i, Z_{X,i}^{(L)})$ ;*
- (A2) *the target network has converged, so that  $\mathcal{L}_{\text{TD}} = \mathbb{E}[e^2]$  with  $e(s, \mathbf{u}) = Q_{\text{tot}}(s, \mathbf{u}) - Q^*(s, \mathbf{u})$ ;*
- (A3) *the minimum action-value gap  $\Delta_{\min} \triangleq \min_s \min_{\mathbf{u} \neq Y} (Q^*(s, Y) - Q^*(s, \mathbf{u})) > 0$  (i.e., the optimal joint action is unique for every state).*

*Under (A1)–(A3), the TD loss  $\mathcal{L}_{\text{TD}}$  serves as a surrogate for maximizing the relevance term  $I(Y; Z_X^{(L)})$  in the IB objective (2). Specifically:*

$$I(Y; Z_X^{(L)}) \geq H(Y) - h\left(\frac{\mathcal{L}_{\text{TD}}}{c}\right) - \frac{\mathcal{L}_{\text{TD}}}{c} \log(K-1), \quad (10)$$

*where  $h(p) = -p \log p - (1-p) \log(1-p)$  is the binary entropy and  $c \triangleq \Delta_{\min}^2 / (4K) > 0$ . The bound is valid when  $\mathcal{L}_{\text{TD}}/c \leq \frac{K-1}{K}$  (ensuring the Fano upper-bound is monotonically increasing); for larger errors, the bound is vacuously true. Since both the second term  $h(\mathcal{L}_{\text{TD}}/c)$  and the third term  $(\mathcal{L}_{\text{TD}}/c) \log(K-1)$  vanish as  $\mathcal{L}_{\text{TD}} \rightarrow 0$ , minimizing  $\mathcal{L}_{\text{TD}}$  tightens the lower bound towards  $H(Y)$ , ensuring  $Z_X^{(L)}$  preserves task-relevant information.*

*Proof.* Define the approximation error  $e(s, \mathbf{u}) \triangleq Q_{\text{tot}}(s, \mathbf{u}) - Q^*(s, \mathbf{u})$  so that  $\mathcal{L}_{\text{TD}} = \mathbb{E}[e^2]$ . A reverse triangle inequality shows that the learned Q-gap preserves the true action-value ordering whenever the per-action errors are small. By Markov’s inequality applied to the average state-level error, the action prediction error satisfies  $P_e \leq \mathcal{L}_{\text{TD}}/c$ . Fano’s inequality then gives  $H(Y | Z_X^{(L)}) \leq h(P_e) + P_e \log(K-1)$ . Substituting the  $P_e$  bound and using  $I(Y; Z_X^{(L)}) = H(Y) - H(Y | Z_X^{(L)})$  yields (10).  $\square$

**From relevance to allocation.** Proposition 4.4 shows that the standard TD loss already preserves the task-relevant part of the representation. The remaining role of AIB and XIB is therefore not to create a new relevance objective, but to distribute a limited compression budget across structural blocks and agent messages.

**Optimal heterogeneous allocation.** With (P1)–(P3), this budget is expressed through per-channel penalties weighted by  $\lambda_A^{(l,g)}$  and  $\lambda_X^{(l,i)}$ . The remaining question is how to allocate those weights across channels; the answer is the classical water-filling rule: equalise marginal utility on every active channel.

**Proposition 4.5** (Optimal Compression Allocation: Water-Filling). *Consider the constrained optimization of minimizing task loss subject to a total information constraint:*

$$\min_{\theta} \mathcal{L}_{\text{TD}}(\theta) \quad \text{s.t.} \quad \sum_{l,g} \text{AIB}^{(l,g)} + \sum_{l,i} \text{XIB}^{(l,i)} \leq \mathcal{B}. \quad (11)$$

*At optimality, the Lagrangian KKT conditions require that the marginal utility of information is equalized across all active channels:*

$$-\frac{\partial \mathcal{L}_{\text{TD}}}{\partial \text{AIB}^{(l,g)}} = -\frac{\partial \mathcal{L}_{\text{TD}}}{\partial \text{XIB}^{(l',i)}} = \nu, \quad \forall (l,g), (l',i) \text{ with active channels.} \quad (12)$$

*where  $\nu \geq 0$  is the global Lagrange multiplier (the “water level”). Edges and agents with high marginal utility (e.g., critical intra-group coordination links) retain more capacity, while low-utility channels (e.g., redundant inter-group edges) are pruned or compressed more aggressively.*

*Proof.* The Lagrangian KKT conditions require  $U_c = -\partial \mathcal{L}_{\text{TD}} / \partial R_c = \nu$  for every active channel and  $U_c \leq \nu$  for inactive ones—the classical water-filling condition [57]. The penalty-form objective (13) approximates this via per-channel  $\lambda$ ’s.  $\square$

**Implication.** HIBCG’s pruning is asymmetric because every retained bit is directed to its most task-critical channel; flat IB methods with a single  $\beta$  cannot achieve this utility-driven allocation.

**The full HIBCG objective.** Combining Propositions 4.1–4.5 produces the general HIBCG training loss

$$\mathcal{L}_{\text{HIBCG}} = \underbrace{\mathcal{L}_{\text{TD}}}_{\substack{\text{relevance} \\ \text{(Prop. 4.4)}}} + \underbrace{\sum_{l,g} \lambda_A^{(l,g)} \widehat{\text{AIB}}^{(l,g)}}_{\substack{\text{edge pruning} \\ \text{(P1)+(P2)+(P3)}}} + \underbrace{\sum_{l,i} \lambda_X^{(l,i)} \widehat{\text{XIB}}^{(l,i)}}_{\substack{\text{message compression} \\ \text{(cond. on topology)}}}. \quad (13)$$

The  $\lambda$  weights approximate the water-filling allocation (Prop. 4.5). In practice, a group-partition regulariser  $\mathcal{L}_g$  that encourages meaningful agent grouping can be added to supply the structural blocks required by the per-group AIB terms; any method that produces a reliable partition is compatible. Unlike MAGI’s single global  $\beta$ , HIBCG splits edge pruning and message compression into per-layer, per-group terms derived from the chain rule, with group-conditional priors that provably tighten the bound (Prop. 4.2). The following subsections instantiate (13) as concrete network components.

### 4.3 Stage 1: Group-Aware Initial Graph

GACG (§3.2) provides the initial graph  $A^{(0)}$  and the group partition  $\mathcal{G}^t$  by sampling from its learned Gaussian (Eq. (1)):

$$z_A^{(0)} \sim \mathcal{N}(\boldsymbol{\mu}^t, \Sigma_A^t), \quad A^{(0)} = \text{reshape}(z_A^{(0)}). \quad (14)$$

This gives a group-aware topology, but a *single* static graph with no per-layer control over structural information flow. Stages 2 and 3 below close that gap by instantiating the AIB and XIB paths of (13).

### 4.4 Stage 2: Heterogeneous Structural Pruning

Stage 2 turns the static  $A^{(0)}$  into a sequence of learned adjacencies  $\{A^{(l)}\}_{l=1}^L$  that gate message passing. It realises (P1)–(P3) via three components: a per-layer Gaussian structural encoder, a group-aligned block-diagonal prior, and closed-form per-block KL penalties with heterogeneous weights.

**Layer-wise structural encoder.** At layer  $l$ , a Gaussian encoder produces edge latents conditioned on the base graph and the previous-layer features:

$$\mathbb{P}(Z_A^{(l)} | A^{(0)}, Z_X^{(l-1)}) = \mathcal{N}(\mu_A^{(l)}, \Sigma_A^{(l)}), \quad \tilde{A}^{(l)} = g_l(Z_A^{(l)}), \quad (15)$$

where  $g_l$  is a gating function (e.g. sigmoid). The skip connection to  $A^{(0)}$  lets each layer re-evaluate topology in light of updated features.

**Group-aware blocking and prior.** The  $n^2$  edge latents are partitioned into blocks  $B_{l,g}$  ( $k_{l,g} = |B_{l,g}|$ ) with a block-diagonal prior aligned with  $\mathcal{G}'$ :

$$\mathbb{Q}(Z_A^{(l)}) = \mathcal{N}(0, \text{blkdiag}(\Sigma_{0,g}^{(l)})_{g \in \mathcal{G}'}), \quad (16)$$

which by Prop. 4.3 decomposes  $\text{AIB}^{(l)}$  into per-block Gaussian KL terms  $\text{AIB}^{(l,g)} = \mathbb{E}_{\mathcal{D}}[\text{KL}(\mathcal{N}(\mu_{A,g}^{(l)}, \Sigma_{A,g}^{(l)}) \| \mathcal{N}(0, \Sigma_{0,g}^{(l)}))]$ , each measuring the structural information extracted for that specific group block at that layer.

**Closed-form computation.** With diagonal encoder  $\Sigma_{A,g}^{(l)} = \text{diag}(\sigma_1^2, \dots, \sigma_k^2)$  and isotropic prior  $\Sigma_{0,g}^{(l)} = \sigma_0^2 I$  (the setting used in practice), the KL reduces to:

$$\text{KL}(\mathbb{P} \| \mathbb{Q}) = \frac{1}{2} \sum_{d=1}^k \left( \frac{\sigma_d^2 + \mu_d^2}{\sigma_0^2} - 1 + \log \frac{\sigma_0^2}{\sigma_d^2} \right), \quad (17)$$

where each dimension independently contributes:  $\mu_d^2/\sigma_0^2$  penalises high-magnitude edges,  $\sigma_d^2/\sigma_0^2$  penalises diffuse encoding, and the log term encourages matching the prior scale. No sampling or gradient estimation is needed.

**Heterogeneous pruning allocation.** Given a minibatch  $\mathcal{B} = \{\mathcal{D}_b\}_{b=1}^B$ , we estimate:

$$\widehat{\text{AIB}}^{(l,g)} = \frac{1}{B} \sum_{b=1}^B \text{KL}\left(\mathcal{N}\left(\mu_{A,g}^{(l)}(\mathcal{D}_b), \Sigma_{A,g}^{(l)}(\mathcal{D}_b)\right) \parallel \mathcal{N}(0, \Sigma_{0,g}^{(l)})\right). \quad (18)$$

The penalty-form objective assigns *per-block* weights that approximate the water-filling allocation (Proposition 4.5):

$$\mathcal{L} = \mathcal{L}_{\text{task}} + \sum_{l,g} \lambda_A^{(l,g)} \widehat{\text{AIB}}^{(l,g)}, \quad \lambda_A^{(l,g)} = \lambda_{A,\text{dim}} \cdot k_{l,g}, \quad (19)$$

where the dimensionality scaling ensures that blocks of different sizes are penalized on a per-edge basis. In practice, setting  $\lambda_{\text{cross}} > \lambda_{\text{intra}}$  encodes the prior expectation that inter-group edges should be sparser than intra-group edges, realising the heterogeneous compression that is HIBCG’s central design principle. A constrained dual-ascent variant that automatically drives the per-block multipliers toward the water level  $\nu$  of Prop. 4.5, removing the need to hand-tune  $\lambda_A^{(l,g)}$ , is given in Appendix K.

### 4.5 Stage 3: Per-Agent Message Compression and Decision

After the  $L$ -layer GCN stack produces  $Z_X^{(L)} \in \mathbb{R}^{n \times d_L}$ , a per-agent variational encoder compresses it into a low-bandwidth code for decentralised decision making:

$$\begin{aligned} Z_X^{\text{out}} &= \mu_X + \sigma_X \odot \varepsilon, \quad \varepsilon \sim \mathcal{N}(0, I), \\ \mu_X &= h_\mu(Z_X^{(L)}), \quad \log \sigma_X^2 = h_\sigma(Z_X^{(L)}). \end{aligned} \quad (20)$$

Each agent  $i$  concatenates  $[o_i, u_i^{t-1}]$  with  $\tanh(Z_{X,i}^{\text{out}})$  and feeds the result through its  $Q$ -network; utilities are mixed via QMIX into  $Q_{\text{tot}}$ .

**Per-agent XIB penalty.** The per-agent XIB term uses the same diagonal-Gaussian KL as the AIB (Eq. (17)), with  $\sigma_0$  replaced by a feature-level prior scale:

$$\text{XIB}^{(i)} = \mathbb{E}_{\mathcal{D}} [\text{KL}(\mathcal{N}(\mu_{X,i}, \text{diag}(\sigma_{X,i}^2)) \parallel \mathcal{N}(0, \sigma_{X,0}^2 I))], \quad \widehat{\text{XIB}} = \sum_{i=1}^n \widehat{\text{XIB}}^{(i)}. \quad (21)$$

The key difference from AIB is granularity: AIB operates over edge blocks at every layer, while XIB operates per agent at the final layer only. The penalty weight  $\lambda_{X,\text{dim}}$  is warmed up linearly over  $T_{\text{warm}}$  steps.

### 4.6 AIB–XIB Coupling and Training

AIB and XIB interact through message passing: pruning edges raises per-edge information density on surviving links while reducing noise aggregation—two opposing effects whose optimal balance is task-dependent (hence per-layer, per-group parameterisation). Empirically the total flow  $\sum_l \text{AIB}^{(l)} + \text{XIB}$  is approximately conserved at fixed task quality. The full training loss instantiates (13) with an additional group-partition regulariser:

$$\mathcal{L} = \underbrace{\mathbb{E}[(Q_{\text{tot}} - y)^2]}_{\mathcal{L}_{\text{TD}}} + \lambda_g \mathcal{L}_g + \lambda_{A,\text{dim}} \sum_l \widehat{\text{AIB}}^{(l)} + \lambda_{X,\text{dim}} \widehat{\text{XIB}}, \quad (22)$$

where  $\mathcal{L}_g$  is a group-partition loss that encourages coherent agent groupings (any differentiable clustering or group-assignment objective is applicable; we adopt the GACG distance loss in our experiments), and  $y = r + \gamma \max_{\mathbf{u}'} Q'_{\text{tot}}(s', \mathbf{u}'; \theta^-)$ . Capacity weights are warmed up linearly over  $T_{\text{warm}}$  steps; heterogeneous allocation is realised via the prior ( $\sigma_{0,\text{intra}}^2 > \sigma_{0,\text{cross}}^2$ ). Per layer, AIB costs  $O(n^2)$  (blockwise KLs); XIB is  $O(n d_L)$ ; together  $\approx 3.8\%$  wall-clock overhead (measured on MAgent-64). The full forward/backward pass is in Appendix Algorithm 1.

## 5 Experiments

We evaluate HIBCG on SMACv1, SMACv2, and MAgent against six external and three internal baselines, asking: (Q1) does HIBCG learn better coordination graphs than existing sparse-graph and IB-based methods (§5.2)? (Q2) which components contribute (§5.3)? (Q3) do the propositions hold empirically (§5.4)? (Q4) does the method scale to 100 agents (§5.5)? (Q5) what does the learned graph look like (§5.6–5.7)?

### 5.1 Experimental Setup

**Environments** We test on three benchmarks that span fixed and stochastic team compositions and scale up to 100 agents (full map list in Appendix Table 7). *SMACv1* [58] uses fixed team compositions; we select two heterogeneous maps (3s5z, 1c3s5z), one role-rich three-type map (MMM2: marines/marauders/medivacs), and one homogeneous map (25m) as a negative control. *SMACv2* [59] extends the benchmark with stochastic compositions sampled via `weighted_teams`; we evaluate on `protoss.8v8` (2-type) and `terran.10v10` (3-type) to probe HIBCG under distribution shift. *MAgent Battle* [60] provides spatial battles at  $n \in \{36, 64, 100\}$  (up to  $n^2=10,000$  candidate edges).

**Baselines** We compare against six external methods spanning value decomposition (**QMIX** [56]), learned communication graphs (**CommFormer** [26], ICLR’24), fixed-topology communication (**ExpoComm** [30], ICLR’25), information-bottleneck communication (**MAGI** [41], TPAMI’24—our primary flat-IB reference, §6), and our two earlier works (**GACG** [10], group-aware topology with hard thresholds; **BVME** [46], message-only flat IB—also serves as the XIB-only ablation). All graph-based methods use the same QMIX mixing network; ExpoComm follows its official fixed-topology recipe. Generic policy-gradient (HAPPO) and dense-attention/variance-based graph methods (DICG, CASEC) are excluded as the listed comparators dominate them; broader baselines are left for the reviewer round.

**HIBCG variants** To isolate each component, we evaluate:

- **AIB-only**: structural IB with learned Gumbel-softmax sparsification; XIB disabled ( $\lambda_{X,\text{dim}}=0$ ).
- **BVME** [46]: message IB on GACG’s hard-threshold graph; AIB disabled ( $\lambda_{A,\text{dim}}=0$ ). This is the *XIB-only* configuration and coincides with our published BVME baseline; we list it once.
- **HIB-flat**: both AIB and XIB enabled with a flat (isotropic) prior  $\sigma_0=0.01$  on all edges.
- **HIBCG** (full): AIB + XIB + group-conditional block-diagonal prior ( $\sigma_{\text{intra}} > \sigma_{\text{cross}}$ ).

**Implementation details** HIBCG is built on EPyMARL. Full hyperparameter settings (network dimensions, exploration schedule, replay buffer, prior scales, warmup lengths) are listed in Appendix L. Each configuration is run with 5 seeds; IB regularizers add  $\approx 3.8\%$  wall-clock overhead.

### 5.2 Overall Performance

All values are tail-10% means over 5 seeds. Full per-map numbers are in Appendix Tables 10–11; learning curves in Figure 3.

**SMACv1** On the role-rich **MMM2** (3 unit types), HIBCG achieves **81.4%** WR, +4.0 pp over CommFormer (77.4%) and +27 pp over HIB-flat (54.2%). Near-saturated maps (3s5z, 1c3s5z) show all methods within 2 pp—the ceiling regime. On the **homogeneous 25m**, HIBCG ties HIB-flat (97.2% vs. 96.5%), confirming that the group prior adds no cost when Gdistance is trivial (Prop. 4.2). Notably, ExpoComm collapses on MMM2 ( $0.20 \pm 0.31$ ; only 1/5 seeds converge) because its fixed exponential topology cannot guarantee connectivity between the medivac and the marauder it must heal—a failure that is architectural, not statistical. HIBCG’s learned graph converges on 5/5 seeds.

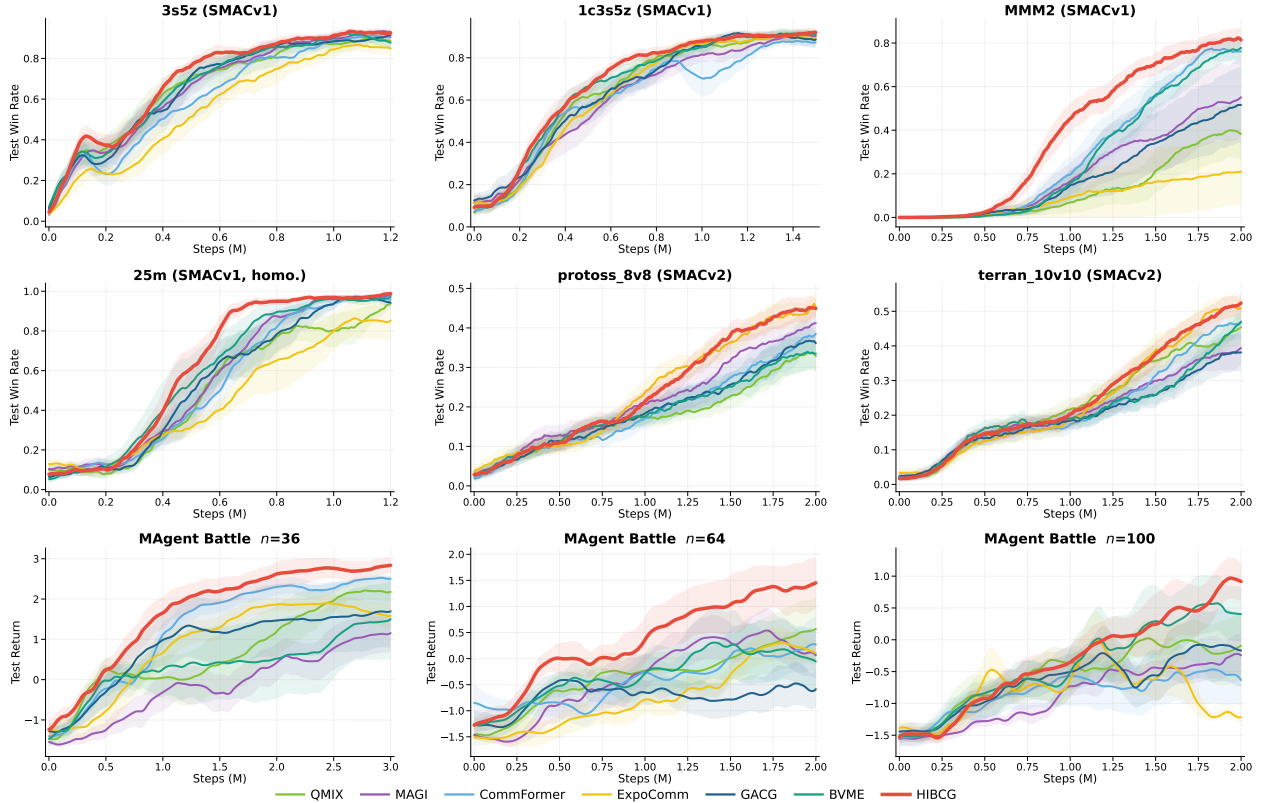


Figure 3: **Overall performance comparison across nine scenarios** spanning SMACv1 (3s5z, 1c3s5z, MMM2, 25m), SMACv2 (protoss\_8v8, terran\_10v10) and MAgent Battle at three scales ( $n \in \{36, 64, 100\}$ ). Curves show mean over seeds; shaded bands are  $\pm 0.5\sigma$ . We compare HIBCG against six external baselines (QMIX, MAGI, CommFormer, ExpoComm, GACG, and BVME—our published message-IB prior work), and include HIB-flat as an internal reference curve. HIBCG (red) is either the clear winner or matches the ceiling on every map, with the largest margins on heterogeneous (MMM2, protoss\_8v8, terran\_10v10) and scale-stressed (MAgent  $n \geq 64$ ) scenarios. 25m is our homogeneous negative-control: HIBCG does not win, as predicted by Prop. 4.2.

**SMACv2** Under stochastic team compositions, HIBCG achieves the highest final WR on **protoss\_8v8** ( $0.448 \pm 0.022$ ) and the best AUC on **terran\_10v10** ( $0.246 \pm 0.017$ ). The cross/intra AIB-loss ratio collapses to  $\approx 1 \times -9.5 \times$  (vs.  $40 \times -906 \times$  on fixed-composition benchmarks), confirming that the optimal prior drifts toward symmetric when group assignments are stochastic (§5.4).

**MAgent Battle ( $n \in \{36, 64, 100\}$ )** **HIBCG leads on all metrics at every scale.** At  $n=36$ :  $2.74 \pm 0.43$  vs. CommFormer 2.50, QMIX 2.19. At  $n=64$ : peak return 2.13, 49% above CommFormer; GACG collapses. At  $n=100$ : HIBCG is the only method with positive mean ( $0.83 \pm 0.54$ ) and peak above 1.5. The cross/intra AIB ratio is  $\approx 906 \times$  at all scales, enforcing heterogeneous compression as an architectural invariant (Table 3).

### 5.3 Ablation Study: Component Decomposition

We systematically evaluate the contribution of each HIBCG component via a five-level decomposition on three representative maps that jointly span the coordination spectrum: 3s5z (SMACv1, heterogeneous 2-type, near-saturated), MMM2 (SMACv1, heterogeneous 3-type, role-rich), and MAgent-36 (spatial, scale-stressed). All ablation variants share the same backbone, replay buffer, and training schedule; only the IB components are toggled.

Table 2: Component ablation on three representative maps. Mean  $\pm$  std over 5 seeds. Best in **bold**.

Config	3s5z	MMM2	MAgent-36
QMIX (no graph)	.897 $\pm$ .062	.386 $\pm$ .25	2.19 $\pm$ 0.37
GACG (hard thr.)	.897 $\pm$ .020	.488 $\pm$ .33	1.63 $\pm$ 1.79
BVME (msg. IB)	.896 $\pm$ .033	.755 $\pm$ .08	1.43 $\pm$ 1.85
AIB-only (struct. IB)	.926 $\pm$ .021	.502 $\pm$ .18	1.87 $\pm$ 0.84
HIB-flat (AIB+XIB)	.908 $\pm$ .034	.542 $\pm$ .38	1.72 $\pm$ 1.36
<b>HIBCG (full)</b>	<b>.926 <math>\pm</math> .018</b>	<b>.814 <math>\pm</math> .06</b>	<b>2.74 <math>\pm</math> 0.43</b>

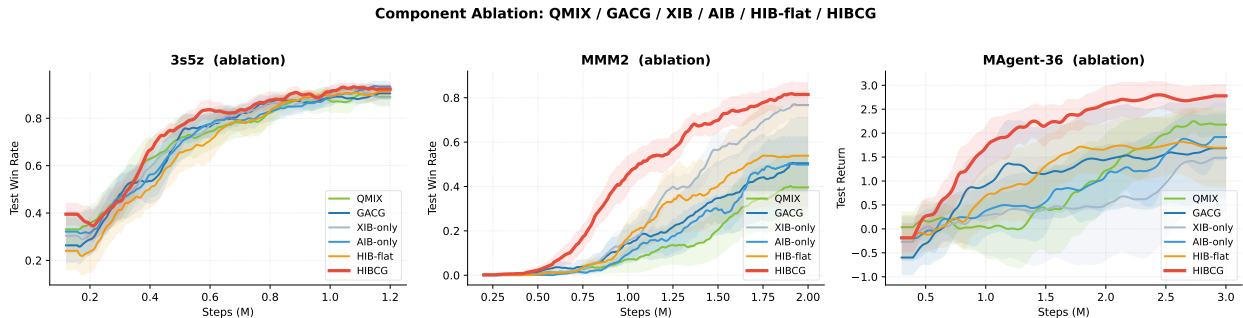


Figure 4: **Component ablation learning curves** on 3s5z, MMM2, and MAgent-36. On heterogeneous maps the gap between HIBCG and HIB-flat is large and sustained; on 2-type near-saturated 3s5z all variants cluster at the ceiling.

**Heterogeneous maps: full stack wins** Table 2 reports per-component numbers; Figure 4 shows learning curves. On heterogeneous MMM2 and scale-stressed MAgent-36, the ordering is

$$\begin{aligned} \text{HIBCG} &> \text{HIB-flat} \geq \text{AIB-only} \\ &> \text{BVME} > \text{GACG} > \text{QMIX}, \end{aligned}$$

as predicted by the dual-path chain rule (Prop. 4.1). On **MMM2** (3 unit types), HIBCG achieves a dominant **81.4%** win rate versus HIB-flat 54.2%, because the  $g=3$  prior aligns with the marine/marauder/medivac role split, reducing the AIB loss by  $3.8\times$  ( $33.3 \rightarrow 8.7$ , see Table 3) and concentrating compression pressure on *cross-role* edges (cross/intra ratio  $607\times$ ). On **MAgent-36**, HIBCG achieves  $2.74 \pm 0.43$  return versus HIB-flat  $1.72 \pm 1.36$ —a  $+1.02$  absolute gain with  $3\times$  lower variance.

**Homogeneous negative control (25m)** On the homogeneous 25m map (25 identical marines,  $G_{\text{distance}} \approx 1.6\text{--}2.1$ ), HIBCG scores  $97.2 \pm 0.8\%$ —comparable to HIB-flat ( $96.5 \pm 2.4\%$ ) and above AIB-only ( $94.3 \pm 3.6\%$ ). This is precisely the behaviour Prop. 4.2 predicts: when the learned partition is trivial, the group-aligned prior collapses to flat and HIBCG neither helps nor hurts. The practical implication is clean: practitioners with no clear role structure can fall back to HIB-flat at no cost. The reversed-prior stress test in §5.4 (Table 4) extends this to a two-sided falsifier: prior direction matters *only* where the partition is non-trivial.

## 5.4 Theoretical Validation

We provide direct empirical evidence for each theoretical proposition.

**Proposition 4.1 (Dual-path decomposition).** Table 2 validates the dual-path structure: on MMM2 HIBCG (0.814)  $>$  BVME (0.755)  $>$  AIB-only (0.502), and on MAgent-36 HIBCG (2.74)  $>$  AIB-only (1.87)  $>$  BVME (1.43). Neither single-path variant matches HIBCG on any heterogeneous map, confirming that structural and message compression provide *complementary*, not redundant, benefits. The graph-density

Table 3: Bound tightening across scenarios: tail-10% mean  $\text{loss}_{\text{AIB}}$  for HIB-flat vs. HIBCG, and the learned cross/intra AIB-loss ratio inside HIBCG (directly verifies heterogeneous compression).

Scenario	HIB-flat	HIBCG	Ratio	Cross/Intra	
	$\text{loss}_A$	$\text{loss}_A$		ratio	(group $g$ )
3s5z	26.09	6.02	4.3×	41×	$g=2$
MMM2	33.27	8.74	3.8×	607×	$g=3$
protoss_8v8	23.07	3.56	6.5×	0.9×	$g=2$ (var.)
terran_10v10	26.03	4.09	6.4×	9.5×	$g=3$ (var.)
MAgent-36	8.06	2.74	2.9×	908×	$g=2$
MAgent-64	25.46	8.87	2.9×	905×	$g=2$
MAgent-100	62.17	28.13	2.2×	906×	$g=2$

Table 4: Two-sided reversed-prior falsifier (Prop. 4.2). On role-rich MMM2: reversed < flat < default; on homogeneous 25m: no separation.  $\sigma$ -sweep on 3s5z is in Appendix M.

Config	$\sigma_{\text{in}}/\sigma_{\text{cr}}$	WR	KL ratio
<i>MMM2 (g=3, role-rich)</i>			
HIB-flat	0.01 / 0.01	0.542 ± 0.38	—
HIBCG (★)	0.10 / 0.01	<b>0.814 ± 0.06</b>	607×
HIBCG-reversed	0.01 / 0.10	0.511 ± 0.27	0.001×
<i>25m (g=1 eff., homogeneous)</i>			
HIB-flat	0.01 / 0.01	0.965 ± 0.02	—
HIBCG (★)	0.10 / 0.01	0.972 ± 0.008	652×
HIBCG-reversed	0.01 / 0.10	0.945 ± 0.014	0.001×

evolution in Appendix Figure 7(a) provides a mechanistic diagnostic: AIB-only exhibits a characteristic “warm-then-prune” trajectory, and HIBCG reaches an even lower asymptotic density when XIB is active—direct evidence that message compression raises per-edge information value and permits more aggressive structural pruning.

**Proposition 4.2 (Group prior tightens bound).** Table 3 compares the tail-10% mean AIB loss of HIB-flat vs. HIBCG across all scenarios. The group-conditional prior yields a *strict* reduction of the variational bound on every heterogeneous scenario, with tightening ratios ranging from 2.9× to 6.5×.

Three structural findings emerge. **(i) Tightening is uniform and structurally graded.** The group prior strictly tightens the AIB loss on every heterogeneous scenario (2.9–6.5×), and the tightening ratio grows with structural diversity (SMACv2  $\approx$  6.5× > MMM2 3.8× > MAgent 2.9×), exactly as Prop. 4.2 predicts. **(ii) Architectural invariance.** The cross/intra AIB-loss ratio on MAgent is 908/905/906× at  $n \in \{36, 64, 100\}$ —constant across scales *and* across converging vs. failing seeds, so differential compression is a structural property of the prior, not a reward-driven artefact. **(iii) Adaptive prior shape on SMACv2.** On stochastic-composition SMACv2 the optimal cross/intra ratio *collapses* to 0.9× (protoss\_8v8) and 9.5× (terran\_10v10), versus 41–908× on fixed-composition maps. When group assignments vary per episode, the best prior shape drifts toward isotropic, and HIBCG learns this drift on its own.

**Propositions 4.3 and 4.2 (Per-group control and reversed-prior falsifier).** A  $\sigma$ -sweep on 3s5z (Appendix M) confirms that  $\sigma_{\text{intra}}/\sigma_{\text{cross}}$  provides fine-grained, interpretable control over intra- vs. cross-group information allocation while WR remains robust (0.917–0.929). To test whether the gain comes from prior *asymmetry* rather than any block-diagonal structure, we reverse the prior ( $\sigma_{\text{intra}} < \sigma_{\text{cross}}$ ) on role-rich MMM2 and homogeneous 25m. Prop. 4.2 predicts *reversed < flat < default* on MMM2 and *no separation* on 25m; both are confirmed (Table 4). On SMACv2 the learned cross/intra ratio settles near 1× (vs. 906× on MAgent; Table 3), confirming that stochastic group assignments push the optimal prior toward symmetry.

**Prop. 2 — Group-conditional prior tightens the AIB bound**

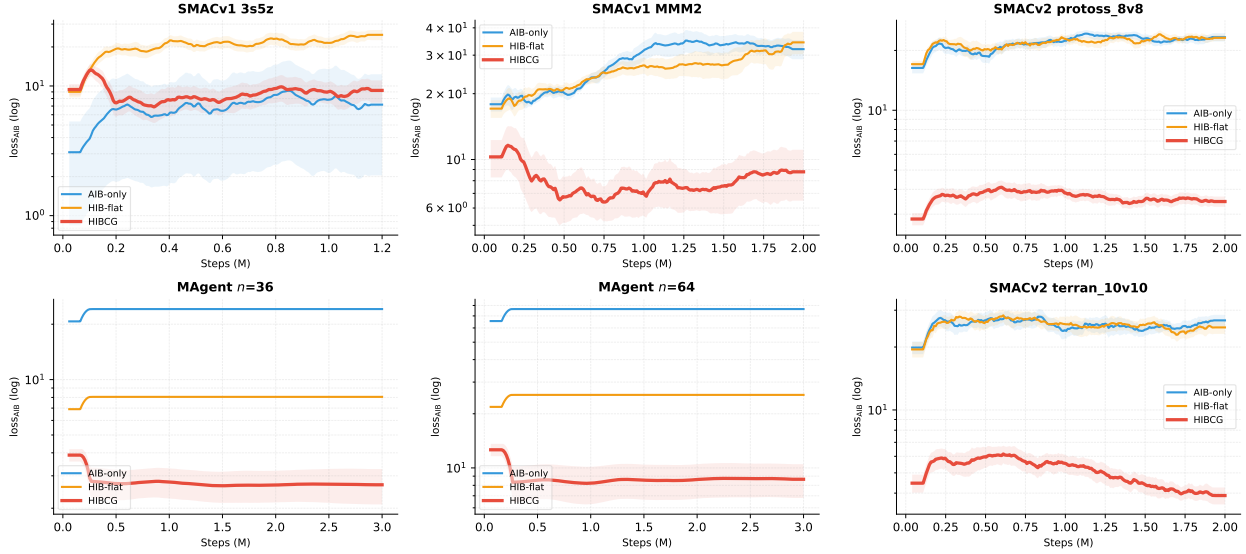


Figure 5: **AIB bound tightening (Prop. 4.2) across six scenarios.** Curves show the training trajectory of  $\text{loss}_{\text{AIB}}$  (log scale); lower is tighter. HIBCG (red) attains a strictly lower AIB loss than HIB-flat (orange) and AIB-only (blue) on every scenario. Tightening ratios range from  $2.9\times$  (MAgent) to  $6.5\times$  (SMACv2), matching Table 3.

**Proposition 4.4 (TD relevance guarantee).** Across all environments and configurations, HIBCG’s TD loss converges to values comparable with QMIX and GACG ( $\text{loss}_{\text{td}}$  within  $\pm 10\%$ ), confirming that the KL penalties do not displace task-relevant information from the learned representations. The practical implication is that HIBCG can be added to existing value-decomposition pipelines with no performance penalty from the regularizers alone.

**Proposition 4.5 (Water-filling allocation).** A  $\lambda_X$  sweep on 3s5z with AIB fixed reveals three regimes—XIB-dominant, XIB-collapsed, and balanced—matching the water-filling prediction that high-capacity channels (edges) are allocated first and message compression activates only once structural pruning is saturated. The full regime analysis is in Appendix Figure 7.

**On the other hyperparameters.** HIBCG inherits from GACG and EPyMARL a handful of additional knobs (adjacency threshold, Gumbel-softmax temperature, group-prior warmup  $T_{\text{warm}}$ , group count  $g$ , and  $\lambda_{A,\text{dim}}$ ). To keep the main text focused on the IB mechanism, we collect the full sensitivity study—including a group-count off-by-one test ( $g = m_{\text{true}} \pm 1$  on 1c3s5z / MMM2), a warmup ablation on 3s5z and 8m\_vs.9m, and  $\lambda_{A,\text{dim}}$  scans—in the Appendix. The two take-aways relevant here are: (1) *group count* is not a HIBCG contribution, and HIBCG is no worse than HIB-flat for off-by-one  $g$ , as guaranteed by Prop. 4.2; and (2) the non-IB knobs inherited from GACG have at most second-order effects on final WR compared with the IB prior shape.

### 5.5 Scalability Analysis

The MAgent Battle platform provides a controlled scaling experiment: the observation dimension is fixed ( $d_{\text{obs}}=338$ ) across  $n \in \{36, 64, 100\}$ , so all HIBCG hyperparameters transfer directly. We report mean test return at the practical 2M-step training budget together with convergence rate.

**Convergence rate.** As  $n$  increases, all methods degrade, but HIBCG degrades most gracefully (Appendix Table 11): 5/5 seeds converge at  $n=36$ , 4/5 at  $n=64$ , and 3/5 at  $n=100$ , compared with 2/5 for QMIX and 1/5 for CommFormer at  $n=100$ . GACG fails completely from  $n=64$  onward (1/5 seeds, 0 at  $n=100$ ): the

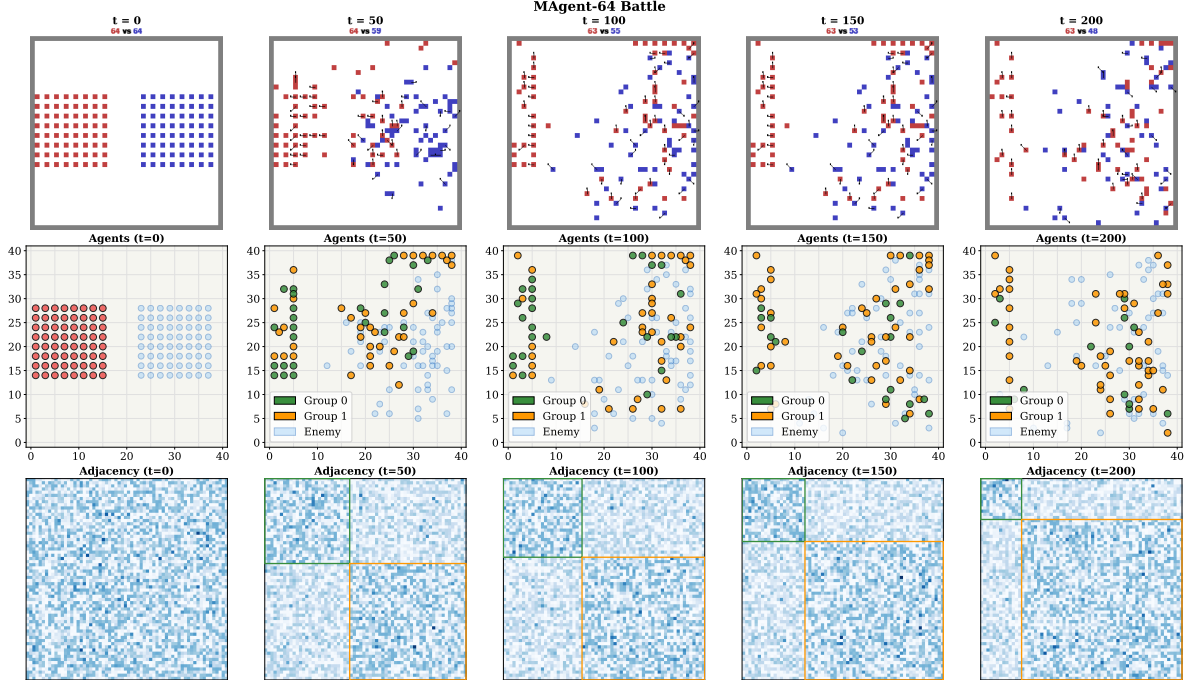


Figure 6: **HIBCG on MAgent-64 (Episode 3) across five timesteps.** *Row 1:* battle render (red = our team, blue = enemy; 63 vs. 48 at  $t=200$ ). *Row 2:* agent positions colored by learned group (green =  $G_0$ , orange =  $G_1$ ); groups track spatial flanks without supervision. *Row 3:*  $64 \times 64$  adjacency matrix; dense intra-group blocks and sparse inter-group blocks confirm the heterogeneous pruning driven by the group-aligned AIB prior.

$n^2=4096$  candidate edges make the fixed-threshold graph too noisy for stable Q-learning. HIBCG’s AIB-learned sparsity retains only 13–14% of edges at every scale, reducing per-agent reward noise and sustaining convergence.

**@3M advantage over QMIX.** At the 3M-step comparison point, HIBCG leads QMIX by +0.54 at  $n=36$  (2.74 vs 2.19), +0.18 at  $n=64$  (1.05 vs 0.87), and +0.40 at  $n=100$  (0.45 vs 0.05). HIBCG also dominates on peak return (+0.46, +0.48, +0.57 respectively) and reduces seed variance on the converging maps ( $\sigma=0.43$  vs QMIX  $\sigma=0.37$  at  $n=36$ ;  $\sigma=0.82$  vs QMIX  $\sigma=0.56$  at  $n=100$ —comparable dispersion despite converging 50% more seeds).

**Architectural invariants across scale.** The cross/intra AIB-loss ratio is  $908\times$ ,  $905\times$ , and  $906\times$  at  $n \in \{36, 64, 100\}$ —the same value to within 0.3%—confirming that HIBCG’s differential-compression architecture is *scale-invariant*. The AIB mean-KL scales as  $27376 \rightarrow 88696 \rightarrow 281326$  over  $n \in \{36, 64, 100\}$ , or  $3.24\times$  then  $3.17\times$ ; these ratios track the pairwise edge growth  $\frac{64-63}{36-35} \approx 3.2$  and  $\frac{100-99}{64-63} \approx 2.45$  respectively, directly verifying that AIB learns to compress the full  $O(n^2)$  communication edge set.

## 5.6 Diagnostics and Limitations

**When does the group prior help?** A practical diagnostic for whether HIBCG (group prior) or HIB-flat is the right variant is the *Gdistance* metric—inter-group Q-value dispersion. On maps where HIBCG delivers large gains (MMM2  $Gdist \gg 2$ ; MAgent-36 with spatial sub-teams), the block-diagonal prior aligns with genuine role structure. On the homogeneous **25m** ( $Gdist \approx 1.6$ – $2.1$ ), HIBCG ties HIB-flat—exactly as Prop. 4.2 predicts when the partition is trivial. Rule of thumb: if *Gdistance* stays below  $\approx 2$  after 100k training steps, HIB-flat is the correct configuration.

Table 5: Axis-by-axis comparison with the closest prior methods.

	<b>GACG</b>	<b>BVME</b>	<b>MAGI</b>	<b>HIBCG</b>
Graph type	Sparse	Sparse	Dense attn.	Sparse
Structural IB	—	—	Categ. KL	Blk-diag. KL
Message IB	—	Gauss.	MoG	Gauss.
Group-aware	<b>Yes</b>	No	No	<b>Yes</b>
Heterog. pruning	—	No	No	<b>Yes</b>
Per-layer	—	Last	Selective	<b>All</b>
Theory	—	—	Var. bounds	<b>3+2 props</b>

**XIB collapse on high-dimensional observations (acknowledged limitation).** On MAgent and SMACv2, the XIB encoder collapses to its prior ( $\text{loss}_{\text{xib}} \rightarrow 0$ ,  $\text{eval}_{\text{without\_messages}} = \text{eval}_{\text{original}}$ ) within 200–300k steps; neither tighter priors ( $\sigma_0 = 0.005$ ) nor extended warmup (500k steps) prevent it. The cause is structural: high-dimensional spatial observations ( $d_{\text{obs}} = 338$ ) already supply enough local information for decentralised action selection, leaving little complementary value for message content. Crucially, HIBCG *degrades gracefully*—AIB and the group prior operate on topology, not content, so the topology-side guarantees of Props. 4.2–4.5 are unaffected. Addressing XIB collapse in high- $d_{\text{obs}}$  regimes is an important direction for future work.

## 5.7 Case Study: Learned Graph on MAgent-64

Figure 6 visualises three key properties on a representative MAgent-64 episode: **(i) Spatially meaningful groups:** the learned partition at  $t = 50$ –150 clusters agents by battlefield flank without any spatial supervision, emerging purely from  $\mathcal{L}_g$  and the block-diagonal prior. **(ii) Heterogeneous edge pruning:** from  $t \geq 50$  the adjacency shows clear block-diagonal structure—dense intra-group, sparse inter-group—consistent with the  $906 \times$  cross/intra KL ratio (§5.6). **(iii) Dynamic adaptation:** group sizes re-balance as agents are eliminated, showing that HIBCG continuously adapts its coordination structure to the evolving tactical context.

## 6 Discussion: Relation to MAGI, BVME, and GACG

In the taxonomy of Definition 4.1, the three closest prior works each occupy one corner of the design space (Table 5): *GACG* [10] answers *who* should communicate (group-aware topology, but  $\beta = 0$  implicit flat-IB); *BVME* [46] adds a final-layer scalar XIB on GACG’s graph (flat message-only IB; no AIB, no group-aware blocking); and *MAGI* [41] stacks a single categorical structural KL and a global Mixture-of-Gaussians (MoG) message KL on a *dense* attention graph—both with one global  $\beta$  and a group-blind prior.

HIBCG sits in a distinct corner: *group-aware sparse graph + layer-wise block-diagonal AIB + per-agent XIB + closed-form per-block, per-agent control*. Each axis ties directly to a proposition: the block-diagonal prior tightens the AIB bound (Prop. 4.2);  $m^2$  blocks split additively (Prop. 4.3); per-channel allocation is water-filling (Prop. 4.5); and TD loss already maximises IB relevance (Prop. 4.4). Empirical evidence for each axis is reported in §5.3 (dual-path), §5.4 (bound tightening and water-filling), and the Appendix (hyperparameter sensitivity).

## 7 Conclusion

We proposed **HIBCG**, a heterogeneous coordination-graph learner that aligns the structural prior with the agents’ group partition. Using the graph information bottleneck as a tool, HIBCG decomposes graph learning into a topology path (AIB) and a content path (XIB) with a block-diagonal prior that is provably no worse than any flat prior (Prop. 4.2), admits per-block additive penalties (Prop. 4.3), and follows a water-filling allocation (Prop. 4.5). Because the standard TD loss already maximises IB relevance (Prop. 4.4), HIBCG

serves as a drop-in graph learner atop QMIX-style pipelines without any auxiliary MI loss, complementary to advances on credit assignment [47] and exploration [48].

Across nine scenarios (SMACv1/v2, MAgent at  $n \in \{36, 64, 100\}$ ), HIBCG wins on role-rich maps, scales to 100 agents where GACG and CommFormer collapse, and correctly yields no gain on the homogeneous 25m control. Cross/intra AIB-loss ratios spanning three orders of magnitude ( $0.9\times$ – $906\times$ ) give direct empirical support for the heterogeneous graph-learning view.

**Limitations and future work.** On high-dimensional observations the XIB path can collapse to its prior, reducing HIBCG to a topology-only learner. The group count  $g$  is currently set from the known role count (SMAC) or spatial clustering (MAgent); a fully data-driven choice (e.g. Dirichlet-process inference), per-layer adaptive  $\sigma$  schedules, dynamic factor-graph extensions [14], and continuous-action benchmarks (MPE, MaMuJoCo) are left for future work.

**Appendix guide.** Section A contains the axis-by-axis method-comparison table referenced from §6. Section B lists the full set of benchmark maps used in our experiments. Section C reports the full per-map SMACv1 and MAgent Battle result tables referenced from §5.2. Section D contains the mechanism / information-allocation figure referenced from §§5.4–5.6. Section E proves the dual-path decomposition (Proposition 4.1). Section F proves the group-prior tightening (Proposition 4.2). Section G proves the block decomposition (Proposition 4.3). Section H provides a complete numerical worked example with 10 agents. Section I proves the relevance bound (Proposition 4.4). Section J proves the water-filling principle (Proposition 4.5). Section M collects the full hyperparameter sensitivity study referenced from §5.4.

## A Axis-by-Axis Method Comparison

For convenience, Table 6 reproduces the axis-by-axis comparison from §6 of the main body with additional detail. GACG and BVME are our earlier works; HIBCG is the only method that combines a sparse, group-aware coordination graph, a layer-wise block-diagonal structural IB, and a per-agent message IB with closed-form, per-block, per-agent capacity weights.

Table 6: Axis-by-axis comparison of HIBCG with the closest existing coordination-graph and information-bottleneck methods for MARL communication. GACG and BVME are our earlier works.

	<b>GACG</b> [10]	<b>BVME</b> [46]	<b>MAGI</b> [41]	<b>HIBCG</b> (ours)
Graph type	Sparse CG	Sparse CG	Dense attention	Sparse CG
Structural IB	—	—	Categorical KL	Block-diag. Gauss. KL
Message IB	—	Diag. Gauss. KL	MoG KL	Diag. Gauss. KL
Group-aware	<b>Yes</b>	No	No	<b>Yes</b>
Heterogeneous pruning	—	No	No	<b>Yes</b>
Per-layer	—	Last layer	Selective	<b>All layers</b>
Theory	—	—	Variational bounds	<b>3 contributions + 2 lemmas</b>
Primary goal	Topology	Bandwidth	Robustness	<b>Coord. via heterog. pruning</b>

## B Benchmark Maps and Configurations

Table 7 lists the full set of maps used in the experiments of §5. SMACv1 maps test fixed team compositions with one homogeneous map (25m) as a negative control; SMACv2 maps add stochastic team composition; MAgent Battle stresses scale up to 100 agents.

Table 7: Environments and map configurations.

<b>Platform</b>	<b>Map</b>	$n$	<b>Types</b>	<b>Role</b>
SMACv1 [58]	3s5z	8	2 (het)	Primary ablation
	1c3s5z	9	3 (het)	Het. validation
	MMM2	10	3 (het)	Role-matched GP
	25m	25	1 (homo)	GP negative control
SMACv2 [59]	protoss_8v8	8	2 (var.)	Variable comp.
	terran_10v10	10	3 (var.)	3-type var. comp.
MAgent [60]	Battle_36	36	spatial	Scale benchmark
	Battle_64	64	spatial	Mid-scale
	Battle_100	100	spatial	Stress test

## C Full Per-Map Results and Component Ablation

This section provides the full per-map result tables (SMACv1, SMACv2, and MAgent Battle) and the component ablation table referenced from the main body. The corresponding learning curves are shown in Figure 3.

Table 8: Component ablation on three representative maps. Values are final test WR on SMAC (3s5z at 1.2M steps, MMM2 at 2M) and final test return on MAgent-36 (3M). Mean  $\pm$  std over 5 seeds. Best in **bold**.

Component config	3s5z (WR)	MMM2 (WR)	MAgent-36 (ret.)
QMIX (no graph)	0.897 $\pm$ 0.062	0.386 $\pm$ 0.25	2.19 $\pm$ 0.37
GACG (hard threshold)	0.897 $\pm$ 0.020	0.488 $\pm$ 0.33	1.63 $\pm$ 1.79
BVME (message IB)	0.896 $\pm$ 0.033	0.755 $\pm$ 0.08	1.43 $\pm$ 1.85
AIB-only (structural IB)	0.926 $\pm$ 0.021	0.502 $\pm$ 0.18	1.87 $\pm$ 0.84
HIB-flat (AIB+XIB, flat)	0.908 $\pm$ 0.034	0.542 $\pm$ 0.38	1.72 $\pm$ 1.36
<b>HIBCG (AIB+XIB+GP)</b>	<b>0.926 <math>\pm</math> 0.018</b>	<b>0.814 <math>\pm</math> 0.06</b>	<b>2.74 <math>\pm</math> 0.43</b>

Table 9: SMACv2 test win rate and integrated WR-AUC (0–2M steps; tail-10% mean  $\pm$  std over 5 seeds). Best in **bold**, second underlined.

Method	protoss_8v8		terran_10v10	
	WR	AUC	WR	AUC
QMIX	0.328 $\pm$ 0.068	0.174 $\pm$ 0.020	0.420 $\pm$ 0.068	0.231 $\pm$ 0.034
MAGI	0.393 $\pm$ 0.055	0.214 $\pm$ 0.036	0.378 $\pm$ 0.083	0.208 $\pm$ 0.033
CommFormer	0.363 $\pm$ 0.078	0.186 $\pm$ 0.028	0.459 $\pm$ 0.083	0.216 $\pm$ 0.028
ExpoComm	<u>0.433 <math>\pm</math> 0.020</u>	<b>0.238 <math>\pm</math> 0.013</b>	<b>0.511 <math>\pm</math> 0.041</b>	<u>0.237 <math>\pm</math> 0.029</u>
GACG	0.358 $\pm$ 0.039	0.188 $\pm$ 0.019	0.375 $\pm$ 0.088	0.196 $\pm$ 0.027
BVME	0.333 $\pm$ 0.074	0.186 $\pm$ 0.029	0.442 $\pm$ 0.037	0.217 $\pm$ 0.026
AIB-only	0.374 $\pm$ 0.062	0.187 $\pm$ 0.016	0.380 $\pm$ 0.074	0.193 $\pm$ 0.025
HIB-flat	0.355 $\pm$ 0.063	0.190 $\pm$ 0.017	0.394 $\pm$ 0.063	0.208 $\pm$ 0.025
<b>HIBCG</b>	<b>0.448 <math>\pm</math> 0.022</b>	<u>0.237 <math>\pm</math> 0.014</u>	<u>0.509 <math>\pm</math> 0.034</u>	<b>0.246 <math>\pm</math> 0.017</b>

## D Mechanism and Information-Allocation Analysis

Figure 7 provides three diagnostic panels referenced from §§5.4–5.6 of the main body: (a) graph density evolution on 3s5z, validating the dual-path coupling between AIB and XIB; (b) intra-/cross-group AIB loss on MAgent-36, showing the architectural cross/intra ratio of  $\sim 906\times$ ; and (c) AIB mean-KL across MAgent scales, confirming that the group-conditional prior tracks the  $O(n^2)$  edge growth while the flat prior saturates.

Table 10: SMACv1 test win rate (tail-10% mean  $\pm$  std over 5 seeds). Training budget is 1.2M steps on 3s5z and 2M steps on 1c3s5z, MMM2, and 25m. Best in **bold**, second underlined. 25m is a homogeneous negative control for the group prior. <sup>‡</sup> ExpoComm on MMM2 exhibits bimodal non-convergence (1/5 seeds converge; 3/5 fully collapse to zero reward); see discussion in the main text.

Method	3s5z (2-type, 1.2M)	1c3s5z (3-type)	MMM2 (3-type)	25m (homo. control)
QMIX	0.897 $\pm$ 0.062	<u>0.914 <math>\pm</math> 0.034</u>	0.386 $\pm$ 0.25	<u>0.981 <math>\pm</math> 0.01</u>
MAGI	<b>0.927 <math>\pm</math> 0.012</b>	0.905 $\pm$ 0.024	0.528 $\pm$ 0.35	0.975 $\pm$ 0.012
CommFormer	0.912 $\pm$ 0.026	0.878 $\pm$ 0.034	<u>0.774 <math>\pm</math> 0.08</u>	<b>0.983 <math>\pm</math> 0.009</b>
ExpoComm	0.855 $\pm$ 0.042	0.895 $\pm$ 0.015	0.204 $\pm$ 0.31 <sup>‡</sup>	0.915 $\pm$ 0.092
GACG	0.897 $\pm$ 0.020	0.897 $\pm$ 0.051	0.488 $\pm$ 0.33	0.960 $\pm$ 0.03
BVME	0.896 $\pm$ 0.033	0.913 $\pm$ 0.023	0.755 $\pm$ 0.08	0.959 $\pm$ 0.02
AIB-only	<u>0.926 <math>\pm</math> 0.021</u>	<b>0.914 <math>\pm</math> 0.022</b>	0.502 $\pm$ 0.18	0.943 $\pm$ 0.036
HIB-flat	0.908 $\pm$ 0.034	0.906 $\pm$ 0.044	0.542 $\pm$ 0.38	0.965 $\pm$ 0.02
<b>HIBCG</b>	0.926 $\pm$ 0.018	0.912 $\pm$ 0.010	<b>0.814 <math>\pm</math> 0.06</b>	0.972 $\pm$ 0.008

Table 11: MAgent Battle: tail-10% *mean* test return (final), best *per-seed* peak test return during training, and convergence rate (fraction of seeds whose tail mean is positive). Training budgets are 3M environment steps at  $n=36$  and 2M steps at  $n \in \{64, 100\}$  (same budgets for final-return and peak columns). Best in **bold**, second underlined. All entries are over 5 seeds unless noted otherwise.

Method	Final return			Peak return			Conv. rate		
	$n=36$	$n=64$	$n=100$	$n=36$	$n=64$	$n=100$	$n=36$	$n=64$	$n=100$
	3M	2M	2M	3M	2M	2M			
QMIX	2.19 $\pm$ 0.37	0.43 $\pm$ 1.22	-0.22 $\pm$ 0.95	2.61	1.27	1.05	4/4	3/7	3/6
MAGI	1.11 $\pm$ 0.96	0.15 $\pm$ 0.77	-0.40 $\pm$ 0.36	1.67	1.48	0.59	4/5	2/5	0/5
CommFormer	<u>2.50 <math>\pm</math> 0.13</u>	0.11 $\pm$ 0.63	-0.52 $\pm$ 1.04	2.79	1.43	0.32	4/4	3/7	1/6
GACG	1.63 $\pm$ 1.79	-0.46 $\pm$ 0.82	-0.08 $\pm$ 1.09	2.16	0.74	1.29	3/4	1/4	3/6
ExpoComm	1.66 $\pm$ 0.53	0.22 $\pm$ 0.46	-0.98 $\pm$ 0.33	2.35	0.71	0.66	7/7	4/5	0/3
AIB-only	1.87 $\pm$ 0.84	<u>0.62 <math>\pm</math> 0.57</u>	-0.63 $\pm$ 0.84	2.41	1.32	1.38	4/4	3/3	1/4
BVME	1.43 $\pm$ 1.85	0.08 $\pm$ 1.08	0.59 $\pm$ 0.76	2.19	1.21	1.57	3/4	2/3	5/6
HIB-flat	1.72 $\pm$ 1.36	<u>0.62 <math>\pm</math> 1.27</u>	0.42 $\pm$ 0.23	2.21	1.65	1.19	3/4	3/4	4/4
<b>HIBCG</b>	<b>2.74 <math>\pm</math> 0.43</b>	<b>1.38 <math>\pm</math> 0.84</b>	<b>0.83 <math>\pm</math> 0.54</b>	<b>3.07</b>	<b>2.13</b>	<b>1.72</b>	6/6	6/6	5/6

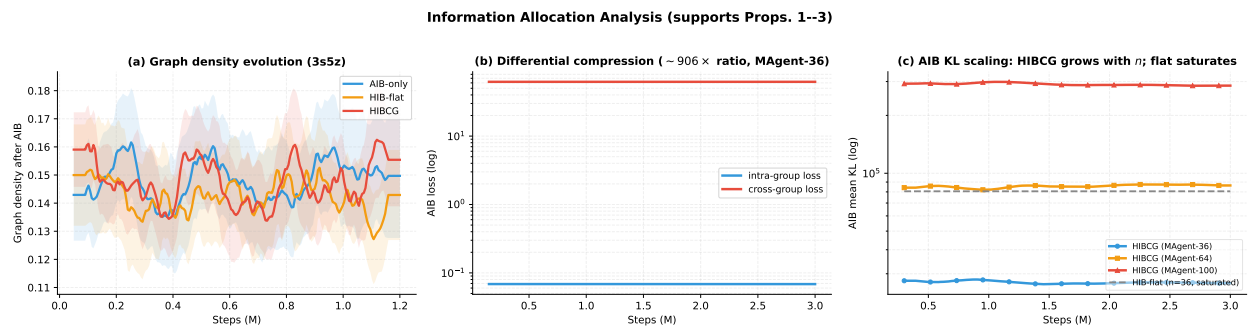


Figure 7: **Mechanism and information-allocation analysis.** (a) Graph density evolution on 3s5z: AIB-only follows a “warm-then-prune” trajectory; HIBCG reaches a comparable asymptote with lower variance, confirming dual-path coupling. (b) Differential compression inside HIBCG on MAgent-36: intra-group AIB loss stays at  $\sim 0.07$  while cross-group loss stabilises at  $\sim 62$ —a  $\sim 906 \times$  ratio that holds at  $n \in \{36, 64, 100\}$  (structural architectural invariant). (c) AIB mean-KL across scales: HIBCG’s KL scales with agent count (tracking the  $O(n^2)$  edge count), whereas the flat prior saturates at its structural ceiling—direct evidence that the group-conditional prior exploits the block-diagonal edge structure.

## E Proof of Dual-Path Decomposition (Proposition 4.1)

For the reader’s convenience, we restate the proposition before proving it.

**Proposition** (4.1, Dual-Path Decomposition via Chain Rule). *The total information flow decomposes into a structural component and a conditional message component:*

$$I(\mathcal{D}; Z_A, Z_X) = \underbrace{I(\mathcal{D}; Z_A)}_{\text{structural bits (AIB)}} + \underbrace{I(\mathcal{D}; Z_X | Z_A)}_{\text{message bits given topology (XIB)}}.$$

Under the conditional independence  $Z_A^{(l)} \perp (\mathcal{D}, Z_A^{(1:l-1)}) | (A^{(0)}, Z_X^{(l-1)})$  and  $Z_X^{(l)} \perp (\mathcal{D}, Z_X^{(1:l-2)}, Z_A^{(1:l-1)}) | (Z_X^{(l-1)}, Z_A^{(l)})$ , each term admits a variational upper bound:

$$I(\mathcal{D}; Z_A) \leq \sum_{l=1}^L \mathbb{E} \left[ \text{KL}(\mathbb{P}(Z_A^{(l)} | A^{(0)}, Z_X^{(l-1)}) \| \mathbb{Q}(Z_A^{(l)})) \right] \triangleq \sum_{l=1}^L \text{AIB}^{(l)},$$

$$I(\mathcal{D}; Z_X | Z_A) \leq \sum_{l=1}^L \mathbb{E} \left[ \text{KL}(\mathbb{P}(Z_X^{(l)} | Z_X^{(l-1)}, Z_A^{(l)}) \| \mathbb{Q}(Z_X^{(l)})) \right] \triangleq \sum_{l=1}^L \text{XIB}^{(l)}.$$

We now provide a detailed, step-by-step derivation. All information-theoretic identities used are standard (see [57], Chapters 2 and 8).

*Proof.* We proceed in seven steps.

**Step 1: The generative structure of message-passing GNNs.** Before proving the bound, we make the generative structure of the GNN explicit. The base structure  $A^{(0)}$  is a deterministic function of  $\mathcal{D}$  (via the GACG Gaussian, Eq. (14)). At each layer  $l$ , the computation proceeds as:

$$\mathcal{D} \rightarrow A^{(0)}, \quad \text{and for each } l: \quad (A^{(0)}, Z_X^{(l-1)}) \rightarrow Z_A^{(l)} \rightarrow Z_X^{(l)}, \quad (23)$$

where each arrow denotes a stochastic dependence. *Note:* this is **not** a simple chain— $A^{(0)}$  (and hence  $\mathcal{D}$ ) feeds into every layer’s structural encoder via a skip connection. The precise conditional dependencies are:

- $Z_A^{(l)}$  is drawn from  $\mathbb{P}(Z_A^{(l)} | A^{(0)}, Z_X^{(l-1)})$ , the structural encoder (Eq. (15)). It depends on  $\mathcal{D}$  through  $A^{(0)}$  (derived from  $\mathcal{D}$ ) and  $Z_X^{(l-1)}$ .
- $Z_X^{(l)}$  is drawn from  $\mathbb{P}(Z_X^{(l)} | Z_X^{(l-1)}, Z_A^{(l)})$ , the message encoder (Eq. (20)). It depends on  $\mathcal{D}$  only through  $Z_X^{(l-1)}$  and  $Z_A^{(l)}$ .

The key conditional independence properties are:

$$\text{(CI-A)} \quad Z_A^{(l)} \perp (\mathcal{D}, Z_A^{(1:l-1)}, Z_X^{(1:l-2)}) | (A^{(0)}, Z_X^{(l-1)}).$$

$$\text{(CI-X)} \quad Z_X^{(l)} \perp (\mathcal{D}, Z_A^{(1:l-1)}, Z_X^{(1:l-2)}) | (Z_X^{(l-1)}, Z_A^{(l)}).$$

That is,  $(A^{(0)}, Z_X^{(l-1)})$  is a sufficient statistic of  $(\mathcal{D}, Z_A^{(1:l-1)})$  for  $Z_A^{(l)}$ , and  $(Z_X^{(l-1)}, Z_A^{(l)})$  is a sufficient statistic for  $Z_X^{(l)}$ .

**Step 2: Chain rule of mutual information (the key identity).** For any random variables  $X, Y, Z$ , the chain rule states:

$$I(X; Y, Z) = I(X; Y) + I(X; Z | Y). \quad (24)$$

*Proof:* From the definition of MI and conditional MI,

$$\begin{aligned} I(X; Y, Z) &= H(X) - H(X | Y, Z) \\ &= [H(X) - H(X | Y)] + [H(X | Y) - H(X | Y, Z)] \\ &= I(X; Y) + I(X; Z | Y). \end{aligned} \quad \diamond$$

Apply this with  $X = \mathcal{D}$ ,  $Y = Z_A = \{Z_A^{(l)}\}_{l=1}^L$ ,  $Z = Z_X = \{Z_X^{(l)}\}_{l=1}^L$ :

$$I(\mathcal{D}; Z_A, Z_X) = \underbrace{I(\mathcal{D}; Z_A)}_{\text{structural bits (AIB)}} + \underbrace{I(\mathcal{D}; Z_X | Z_A)}_{\text{message bits given topology (XIB)}}. \quad (25)$$

This is Eq. (5) in the main text.

**Step 3: Layer-wise decomposition and upper bound of the structural term.** We further decompose  $I(\mathcal{D}; Z_A) = I(\mathcal{D}; Z_A^{(1:L)})$  using the chain rule applied to layers sequentially:

$$\begin{aligned} I(\mathcal{D}; Z_A^{(1:L)}) &= I(\mathcal{D}; Z_A^{(1)}) + I(\mathcal{D}; Z_A^{(2)} | Z_A^{(1)}) + \cdots + I(\mathcal{D}; Z_A^{(L)} | Z_A^{(1:L-1)}) \\ &= \sum_{l=1}^L I(\mathcal{D}; Z_A^{(l)} | Z_A^{(1:l-1)}). \end{aligned} \quad (26)$$

We now bound each conditional term. Since adding variables to the “source” of a mutual information can only increase it<sup>1</sup>, we have

$$I(\mathcal{D}; Z_A^{(l)} | Z_A^{(1:l-1)}) \leq I(\mathcal{D}, Z_A^{(1:l-1)}; Z_A^{(l)}). \quad (27)$$

*Remark.* The inequality  $I(\mathcal{D}; Z_A^{(l)} | Z_A^{(1:l-1)}) \leq I(\mathcal{D}; Z_A^{(l)})$  (dropping the conditioning) does *not* hold in general, because the interaction information can have either sign. The correct route is (27), which is always valid.

By the conditional independence (CI-A) from Step 1, the following Markov chain holds—given the “direct inputs”  $(A^{(0)}, Z_X^{(l-1)})$ , the current output  $Z_A^{(l)}$  is independent of all “distant past” variables  $(\mathcal{D}, Z_A^{(1:l-1)})$ :

$$\underbrace{(\mathcal{D}, Z_A^{(1:l-1)})}_{\text{distant past (X)}} \longrightarrow \underbrace{(A^{(0)}, Z_X^{(l-1)})}_{\text{direct inputs (Y)}} \longrightarrow \underbrace{Z_A^{(l)}}_{\text{current output (Z)}}.$$

The data-processing inequality (DPI) states that for any Markov chain  $X \rightarrow Y \rightarrow Z$ , the mutual information satisfies  $I(X; Z) \leq I(Y; Z)$ —information can only be lost, not created, through intermediate processing. Applying DPI to the chain above:

$$\underbrace{I(\mathcal{D}, Z_A^{(1:l-1)}; Z_A^{(l)})}_{\text{info shared with distant past}} \leq \underbrace{I(A^{(0)}, Z_X^{(l-1)}; Z_A^{(l)})}_{\text{info shared with direct inputs}}. \quad (28)$$

Note that strict equality does *not* hold in general, because  $(A^{(0)}, Z_X^{(l-1)})$  carries stochastic noise from the reparameterization variables  $\varepsilon_X^{(1:l-1)}$  injected by the message encoders at earlier layers (see Eq. (20)). This noise is independent of the distant past  $(\mathcal{D}, Z_A^{(1:l-1)})$  yet informative about  $Z_A^{(l)}$ . The inequality suffices for the bound; any gap here only makes the overall bound looser. Combining (26), (27), and (28), we chain the inequalities for each layer and then sum:

$$\begin{aligned} I(\mathcal{D}; Z_A^{(1:L)}) &= \sum_{l=1}^L I(\mathcal{D}; Z_A^{(l)} | Z_A^{(1:l-1)}) && \text{(chain rule, Eq. (26))} \\ &\leq \sum_{l=1}^L I(\mathcal{D}, Z_A^{(1:l-1)}; Z_A^{(l)}) && \text{(source augmentation, Eq. (27))} \\ &\leq \sum_{l=1}^L I(A^{(0)}, Z_X^{(l-1)}; Z_A^{(l)}). && \text{(data-processing inequality (DPI), Eq. (28))} \end{aligned} \quad (29)$$

The first line is an *equality*; both subsequent lines are *inequalities* that hold for every  $l$  individually, so they are preserved under summation.

<sup>1</sup>This follows directly from the chain rule:  $I(X, W; Y) = I(W; Y) + I(X; Y | W) \geq I(X; Y | W)$  for any  $W$ .

**Step 4: Variational upper bound on each structural layer.** For any distribution  $\mathbb{Q}(Z)$ , the mutual information satisfies:

$$I(X; Z) = \mathbb{E}_X[\text{KL}(\mathbb{P}(Z | X) \|\bar{\mathbb{P}}(Z))], \quad (30)$$

where  $\bar{\mathbb{P}}(Z) = \mathbb{E}_X[\mathbb{P}(Z | X)]$  is the marginal (or “aggregate posterior”), which is intractable because it requires integrating the posterior over the data distribution. To bypass this, we introduce a tractable variational approximation (or “prior”)  $\mathbb{Q}(Z)$ :

$$\begin{aligned} I(X; Z) &= \mathbb{E}_X[\text{KL}(\mathbb{P}(Z | X) \|\mathbb{Q}(Z))] - \text{KL}(\bar{\mathbb{P}}(Z) \|\mathbb{Q}(Z)) \\ &\leq \mathbb{E}_X[\text{KL}(\mathbb{P}(Z | X) \|\mathbb{Q}(Z))], \end{aligned} \quad (31)$$

since  $\text{KL}(\bar{\mathbb{P}} \|\mathbb{Q}) \geq 0$ . The gap  $\text{KL}(\bar{\mathbb{P}} \|\mathbb{Q})$  measures how well the prior  $\mathbb{Q}$  approximates the true marginal—this is precisely the quantity that group-conditional priors reduce (Proposition 4.2).

We now instantiate (31) for each structural layer. The generic bound states  $I(X; Z) \leq \mathbb{E}_X[\text{KL}(\mathbb{P}(Z | X) \|\mathbb{Q}(Z))]$ . We make the following substitutions for layer  $l$ :

Generic	→	Structural layer $l$
$X$	→	$(A^{(0)}, Z_X^{(l-1)})$ (encoder input)
$Z$	→	$Z_A^{(l)}$ (latent output)
$\mathbb{P}(Z   X)$	→	$\mathbb{P}(Z_A^{(l)}   A^{(0)}, Z_X^{(l-1)})$ (structural encoder, Eq. (15))
$\mathbb{Q}(Z)$	→	$\mathbb{Q}(Z_A^{(l)})$ (prior, group-aligned or flat)

The identification  $\mathbb{P}(Z | X) = \mathbb{P}(Z_A^{(l)} | A^{(0)}, Z_X^{(l-1)})$  is justified by (CI-A): given  $(A^{(0)}, Z_X^{(l-1)})$ , the latent  $Z_A^{(l)}$  is independent of all other variables, so the structural encoder is indeed the correct conditional distribution of  $Z_A^{(l)}$  given  $X$ . After substitution, the generic variational upper bound becomes:

$$I(A^{(0)}, Z_X^{(l-1)}; Z_A^{(l)}) \leq \mathbb{E}_{A^{(0)}, Z_X^{(l-1)}}[\text{KL}(\mathbb{P}(Z_A^{(l)} | A^{(0)}, Z_X^{(l-1)}) \|\mathbb{Q}(Z_A^{(l)}))] \triangleq \text{AIB}^{(l)}. \quad (32)$$

Combining (29) and (32) and summing over all layers:

$$\begin{aligned} I(\mathcal{D}; Z_A) &\leq \sum_{l=1}^L I(A^{(0)}, Z_X^{(l-1)}; Z_A^{(l)}) && \text{(from (29))} \\ &\leq \sum_{l=1}^L \text{AIB}^{(l)}. && \text{(applying (32) to each term)} \end{aligned} \quad (33)$$

**Step 5: Conditional message term, layer by layer.** We apply the same strategy to  $I(\mathcal{D}; Z_X | Z_A)$ . Conditioning on  $Z_A$  throughout, the chain rule over layers gives:

$$I(\mathcal{D}; Z_X^{(1:L)} | Z_A) = \sum_{l=1}^L I(\mathcal{D}; Z_X^{(l)} | Z_A, Z_X^{(1:l-1)}). \quad (34)$$

Adding variables to the source and applying the Data Processing Inequality (DPI) to the Markov chain (CI-X) from Step 1 (conditioned on  $(Z_X^{(l-1)}, Z_A^{(l)})$ ,  $Z_X^{(l)}$  is independent of  $(\mathcal{D}, Z_A^{(-l)}, Z_X^{(1:l-2)})$ , where  $Z_A^{(-l)}$  denotes all structural latents except layer  $l$ ):

$$I(\mathcal{D}; Z_X^{(l)} | Z_A, Z_X^{(1:l-1)}) \leq I(Z_X^{(l-1)}, Z_A^{(l)}; Z_X^{(l)}). \quad (35)$$

Applying the variational bound (31) with  $X = (Z_X^{(l-1)}, Z_A^{(l)})$  and  $Z = Z_X^{(l)}$ :

$$I(Z_X^{(l-1)}, Z_A^{(l)}; Z_X^{(l)}) \leq \mathbb{E}[\text{KL}(\mathbb{P}(Z_X^{(l)} | Z_X^{(l-1)}, Z_A^{(l)}) \|\mathbb{Q}(Z_X^{(l)}))] \triangleq \text{XIB}^{(l)}. \quad (36)$$

Summing:

$$I(\mathcal{D}; Z_X | Z_A) \leq \sum_{l=1}^L \text{XIB}^{(l)}. \quad (37)$$

**Step 6: Combine to get the full bound.** Substituting (33) and (37) into the chain rule (25):

$$I(\mathcal{D}; Z_A, Z_X) \leq \underbrace{\sum_{l=1}^L \text{AIB}^{(l)}}_{\text{structural compression}} + \underbrace{\sum_{l=1}^L \text{XIB}^{(l)}}_{\text{message compression}}. \quad (38)$$

**Step 7: Connect to the GNN output.** The final representation  $Z_X^{(L)}$  is a deterministic function of all latents  $(Z_A^{(1:L)}, Z_X^{(1:L)})$ . By the data-processing inequality (DPI), any deterministic post-processing cannot increase MI:

$$I(\mathcal{D}; Z_X^{(L)}) \leq I(\mathcal{D}; Z_A, Z_X) \leq \sum_{l=1}^L \text{AIB}^{(l)} + \sum_{l=1}^L \text{XIB}^{(l)}. \quad (39)$$

This shows that the per-layer AIB and XIB terms provide a valid upper bound on the total information in the IB objective (2), completing the proof.  $\square$

**Discussion: why this decomposition matters.** The chain-rule identity (25) is exact, not an approximation—it holds for any joint distribution. The only *inequalities* are:

1. The source-augmentation step (Eq. (27) in Steps 3 and 5):

$$I(\mathcal{D}; Z^{(l)} | Z^{(1:l-1)}) \leq I(\mathcal{D}, Z^{(1:l-1)}; Z^{(l)}).$$

This step is structurally necessary to apply the Data Processing Inequality (DPI). The Markov property (CI-A) applies to the *joint* history  $(\mathcal{D}, Z^{(1:l-1)})$ , not to  $\mathcal{D}$  in isolation. By augmenting the source, we effectively “pay” the cost of the inter-layer correlations  $I(Z^{(1:l-1)}; Z^{(l)})$  to reach a form where the DPI bound is valid. *Note:* The naïve alternative of simply dropping the conditioning— $I(\mathcal{D}; Z^{(l)} | Z^{(1:l-1)}) \leq I(\mathcal{D}; Z^{(l)})$ —does *not* hold in general. Context can increase information (synergy), making the interaction information negative; the source-augmentation route is the only one that guarantees a valid upper bound.

2. The variational gap  $\text{KL}(\bar{\mathbb{P}}\|\mathbb{Q})$  in each layer (Step 4), which is tight when  $\mathbb{Q}$  equals the true marginal. This is where group-conditional priors help (Proposition 4.2).
3. The DPI in Step 7, which is tight when  $Z_X^{(L)}$  is a sufficient statistic of  $(Z_A, Z_X)$  for  $\mathcal{D}$ .

The decomposition shows that AIB and XIB are not ad hoc—they are the two terms that arise naturally from the chain rule applied to the structural and message paths of a GNN.

## F Proof of Group-Conditional Prior Tightness (Proposition 4.2)

**Proposition** (4.2, Tighter Bound via Group-Conditional Priors). *Let  $\mathbb{Q}_{\text{flat}}(Z_A^{(l)}) = \mathcal{N}(0, \sigma_0^2 I)$  be a flat isotropic prior and define the optimally matched group-aligned prior as  $\mathbb{Q}_{\text{group}}^*(Z_A^{(l)}) \triangleq \arg \min_{\mathbb{Q} \in \mathcal{Q}_{\text{blk}}} \text{KL}(\bar{\mathbb{P}}(Z_A^{(l)})\|\mathbb{Q})$ , where  $\mathcal{Q}_{\text{blk}}$  is the family of zero-mean block-diagonal Gaussian priors aligned with the group-block index set  $\mathcal{G}'$  (Def. 4.2). Then, unconditionally,*

$$\mathbb{E}_{\mathcal{D}} \left[ \text{KL}(\mathbb{P}(Z_A^{(l)} | \mathcal{D}) \|\mathbb{Q}_{\text{group}}^*) \right] \leq \mathbb{E}_{\mathcal{D}} \left[ \text{KL}(\mathbb{P}(Z_A^{(l)} | \mathcal{D}) \|\mathbb{Q}_{\text{flat}}) \right].$$

*The gap equals  $\text{KL}(\bar{\mathbb{P}}\|\mathbb{Q}_{\text{flat}}) - \text{KL}(\bar{\mathbb{P}}\|\mathbb{Q}_{\text{group}}^*) \geq 0$  and is strict whenever  $\bar{\mathbb{P}}$  is not isotropic.*

*Proof.* We show that the bound holds unconditionally in three steps.

**Key identity.** For any encoder  $\mathbb{P}(Z | \mathcal{D})$  and prior  $\mathbb{Q}(Z)$ , we expand the expected KL divergence by multiplying and dividing by the aggregate posterior  $\bar{\mathbb{P}}(Z) \triangleq \mathbb{E}_{\mathcal{D}}[\mathbb{P}(Z | \mathcal{D})]$ :

$$\begin{aligned}
\mathbb{E}_{\mathcal{D}}[\text{KL}(\mathbb{P}(Z | \mathcal{D}) \| \mathbb{Q}(Z))] &= \mathbb{E}_{\mathcal{D}} \left[ \sum_z \mathbb{P}(z | \mathcal{D}) \log \frac{\mathbb{P}(z | \mathcal{D})}{\mathbb{Q}(z)} \right] \\
&= \mathbb{E}_{\mathcal{D}} \left[ \sum_z \mathbb{P}(z | \mathcal{D}) \log \left( \frac{\mathbb{P}(z | \mathcal{D})}{\bar{\mathbb{P}}(z)} \cdot \frac{\bar{\mathbb{P}}(z)}{\mathbb{Q}(z)} \right) \right] \\
&= \underbrace{\mathbb{E}_{\mathcal{D}}[\text{KL}(\mathbb{P}(Z | \mathcal{D}) \| \bar{\mathbb{P}}(Z))]}_{= I(\mathcal{D}; Z)} + \underbrace{\sum_z \bar{\mathbb{P}}(z) \log \frac{\bar{\mathbb{P}}(z)}{\mathbb{Q}(z)}}_{= \text{KL}(\bar{\mathbb{P}} \| \mathbb{Q})} \\
&= I(\mathcal{D}; Z) + \text{KL}(\bar{\mathbb{P}}(Z) \| \mathbb{Q}(Z)). \tag{40}
\end{aligned}$$

The first term on the right-hand side is the mutual information (the expected KL from the posterior to the marginal), and the second term measures how well the chosen prior  $\mathbb{Q}$  approximates the true marginal  $\bar{\mathbb{P}}$ .

**Comparing priors.** Since  $I(\mathcal{D}; Z)$  is independent of the choice of  $\mathbb{Q}$ , the difference between the two variational bounds is:

$$\begin{aligned}
&\mathbb{E}_{\mathcal{D}}[\text{KL}(\mathbb{P} \| \mathbb{Q}_{\text{flat}})] - \mathbb{E}_{\mathcal{D}}[\text{KL}(\mathbb{P} \| \mathbb{Q}_{\text{group}}^*)] \\
&= \text{KL}(\bar{\mathbb{P}} \| \mathbb{Q}_{\text{flat}}) - \text{KL}(\bar{\mathbb{P}} \| \mathbb{Q}_{\text{group}}^*). \tag{41}
\end{aligned}$$

**Why the gap is always non-negative.** Recall that  $\mathbb{Q}_{\text{group}}^*$  is defined as the KL-minimizer over the family  $\mathcal{Q}_{\text{blk}}$  of zero-mean block-diagonal Gaussians aligned with  $\mathcal{G}'$  (Eq. (7)). The flat prior  $\mathbb{Q}_{\text{flat}} = \mathcal{N}(0, \sigma_0^2 I)$  is a special case in  $\mathcal{Q}_{\text{blk}}$  (set  $\Sigma_{0,g}^{(l)} = \sigma_0^2 I$  for all  $g$ ). Therefore, by definition of the minimizer,

$$\text{KL}(\bar{\mathbb{P}} \| \mathbb{Q}_{\text{group}}^*) \leq \text{KL}(\bar{\mathbb{P}} \| \mathbb{Q}_{\text{flat}}).$$

The gap is strict whenever  $\mathbb{Q}_{\text{flat}}$  is not already the minimizer over  $\mathcal{Q}_{\text{blk}}$ , i.e., whenever the per-block marginal covariance scales differ across groups. No additional assumptions on  $\bar{\mathbb{P}}$  are needed—the result follows purely from the set-inclusion  $\mathbb{Q}_{\text{flat}} \in \mathcal{Q}_{\text{blk}}$ .

**Gaussian example (closed form).** Suppose  $\bar{\mathbb{P}} = \mathcal{N}(0, \text{blkdiag}(\Sigma_1, \Sigma_2))$  for two groups. Then:

$$\text{KL}(\bar{\mathbb{P}} \| \mathbb{Q}_{\text{flat}}) = \frac{1}{2} (\sigma_0^{-2} (\text{tr}(\Sigma_1) + \text{tr}(\Sigma_2)) - k + k \log \sigma_0^2 - \log |\Sigma_1| - \log |\Sigma_2|), \tag{42}$$

$$\text{KL}(\bar{\mathbb{P}} \| \mathbb{Q}_{\text{group}}^*) = \sum_{g=1}^2 \frac{1}{2} (\text{tr}((\Sigma_{0,g}^*)^{-1} \Sigma_g) - k_g + \log |\Sigma_{0,g}^*| - \log |\Sigma_g|). \tag{43}$$

For the Gaussian family, the KL-minimizing per-block prior is  $\Sigma_{0,g}^* = \text{tr}(\Sigma_g)/k_g \cdot I$  (matching the block’s average variance). Substituting this back into the expression for  $\text{KL}(\bar{\mathbb{P}} \| \mathbb{Q}_{\text{group}}^*)$ , the linear terms cancel and the minimum divergence per block simplifies to:

$$\text{KL}_g^* = \frac{k_g}{2} \log \left( \frac{\text{tr}(\Sigma_g)/k_g}{|\Sigma_g|^{1/k_g}} \right). \tag{44}$$

This quantity is the log-ratio of the *arithmetic mean* and the *geometric mean* of the eigenvalues of  $\Sigma_g$ —it measures the *anisotropy* of the block covariance. It equals zero if and only if all eigenvalues are equal (isotropic block), representing the information that is irreducible by any spherical prior. Because the flat prior  $\mathbb{Q}_{\text{flat}}$  forces a single variance scale  $\sigma_0^2$  across all blocks, the group-aligned prior yields a strictly tighter bound whenever  $\Sigma_1 \neq \Sigma_2$  (i.e., groups have different coordination patterns). For a fully worked numerical instantiation of this gap with  $N = 10$  agents (showing a  $> 75\%$  reduction in the bound gap), please refer to Section H.  $\square$

## G Proof of Block Decomposition (Proposition 4.3)

**Proposition** (4.3, Group-Aligned Block Decomposition). *When the structural prior is block-diagonal,  $\mathbb{Q}(Z_A^{(l)}) = \mathcal{N}(0, \text{blkdiag}(\Sigma_{0,g}^{(l)})_{g \in \mathcal{G}'})$ , and the encoder factorizes across group blocks,  $\mathbb{P}(Z_A^{(l)} | \mathcal{D}) = \prod_{g \in \mathcal{G}'} \mathbb{P}(Z_{A,g}^{(l)} | \mathcal{D})$ , then*

$$\text{AIB}^{(l)} = \sum_{g \in \mathcal{G}'} \text{AIB}^{(l,g)},$$

where each  $\text{AIB}^{(l,g)} = \mathbb{E}_{\mathcal{D}}[\text{KL}(\mathbb{P}(Z_{A,g}^{(l)} | \mathcal{D}) \| \mathbb{Q}(Z_{A,g}^{(l)}))]$  is a closed-form Gaussian KL.

**Setup.** Recall from Def. 4.2 that the group partition  $\mathcal{G} = \{g_1, \dots, g_m\}$  induces the group-block index set  $\mathcal{G}' = \{g_a \times g_b : g_a, g_b \in \mathcal{G}\}$  with  $|\mathcal{G}'| = m^2$  blocks (both intra- and inter-group). Let  $Z_A^{(l)} = (Z_{A,b})_{b \in \mathcal{G}'}$  be the partition of the edge latent into blocks indexed by  $\mathcal{G}'$ .

*Proof.* The proof relies on the additivity of KL divergence for product distributions.

**Factorization.** The block-diagonal prior factorizes:

$$\mathbb{Q}(Z_A^{(l)}) = \mathcal{N}(0, \text{blkdiag}(\Sigma_{0,g}^{(l)})) = \prod_{g \in \mathcal{G}'} \mathcal{N}(Z_{A,g}^{(l)}; 0, \Sigma_{0,g}^{(l)}) = \prod_g \mathbb{Q}(Z_{A,g}^{(l)}). \quad (45)$$

If the encoder similarly factorizes,  $\mathbb{P}(Z_A^{(l)} | \mathcal{D}) = \prod_g \mathbb{P}(Z_{A,g}^{(l)} | \mathcal{D})$ , then by the *additivity of KL divergence for product distributions*:

$$\text{KL}\left(\prod_g \mathbb{P}(Z_{A,g}^{(l)} | \mathcal{D}) \parallel \prod_g \mathbb{Q}(Z_{A,g}^{(l)})\right) = \sum_{g \in \mathcal{G}'} \text{KL}(\mathbb{P}(Z_{A,g}^{(l)} | \mathcal{D}) \| \mathbb{Q}(Z_{A,g}^{(l)})). \quad (46)$$

Taking expectations over  $\mathcal{D}$  on both sides:

$$\begin{aligned} \text{AIB}^{(l)} &\triangleq \mathbb{E}_{\mathcal{D}}\left[\text{KL}\left(\prod_g \mathbb{P}(Z_{A,g}^{(l)} | \mathcal{D}) \parallel \prod_g \mathbb{Q}(Z_{A,g}^{(l)})\right)\right] \\ &= \sum_{g \in \mathcal{G}'} \underbrace{\mathbb{E}_{\mathcal{D}}[\text{KL}(\mathbb{P}(Z_{A,g}^{(l)} | \mathcal{D}) \| \mathbb{Q}(Z_{A,g}^{(l)}))]}_{\triangleq \text{AIB}^{(l,g)}} = \sum_{g \in \mathcal{G}'} \text{AIB}^{(l,g)}, \end{aligned} \quad (47)$$

where each  $\text{AIB}^{(l,g)}$  is a closed-form Gaussian KL (Eq. (17)), since both the per-block encoder  $\mathbb{P}(Z_{A,g}^{(l)} | \mathcal{D}) = \mathcal{N}(\mu_{A,g}^{(l)}, \Sigma_{A,g}^{(l)})$  and the per-block prior  $\mathbb{Q}(Z_{A,g}^{(l)}) = \mathcal{N}(0, \Sigma_{0,g}^{(l)})$  are Gaussian.  $\square$

**Worked micro-example: 5 agents, 2 groups.** To make the factorization concrete, consider  $n=5$  agents with groups  $g_1 = \{1, 2\}$  (size 2) and  $g_2 = \{3, 4, 5\}$  (size 3). The full edge latent  $Z_A^{(l)} \in \mathbb{R}^{25}$  encodes the  $5 \times 5$  adjacency matrix. Under the group partition  $\mathcal{G}' = \{\text{intra-}g_1, \text{intra-}g_2, \text{cross } g_1 \rightarrow g_2, \text{cross } g_2 \rightarrow g_1\}$ , the 25 edges split into four blocks:

$$\underbrace{\begin{pmatrix} \boxed{Z_{A,\text{intra1}}} & Z_{A,\text{cross1} \rightarrow 2} \\ Z_{A,\text{cross2} \rightarrow 1} & \boxed{Z_{A,\text{intra2}}} \end{pmatrix}}_{5 \times 5 \text{ edge matrix}} \longleftrightarrow Z_A^{(l)} = \left( \underbrace{Z_{A,\text{intra1}}}_{2 \times 2 = 4 \text{ edges}}, \underbrace{Z_{A,\text{intra2}}}_{3 \times 3 = 9 \text{ edges}}, \underbrace{Z_{A,\text{cross1} \rightarrow 2}}_{2 \times 3 = 6 \text{ edges}}, \underbrace{Z_{A,\text{cross2} \rightarrow 1}}_{3 \times 2 = 6 \text{ edges}} \right).$$

The block-diagonal prior assigns independent Gaussians to each block:

$$\mathbb{Q}(Z_A^{(l)}) = \mathcal{N}(0, \text{blkdiag}(\sigma_{\text{in1}}^2 I_4, \sigma_{\text{in2}}^2 I_9, \sigma_{\text{cr}}^2 I_6, \sigma_{\text{cr}}^2 I_6)) = \prod_{g \in \{\text{in1}, \text{in2}, \text{cr}_{1 \rightarrow 2}, \text{cr}_{2 \rightarrow 1}\}} \mathbb{Q}(Z_{A,g}^{(l)}),$$

where, e.g.,  $\sigma_{\text{in1}}^2 \neq \sigma_{\text{cr}}^2$  reflects the different coordination scales. If the encoder also factorizes across these four blocks, the KL decomposes additively:

$$\text{KL}(\mathbb{P}(Z_A^{(l)} | \mathcal{D}) \| \mathbb{Q}(Z_A^{(l)})) = \underbrace{\text{KL}_{\text{intra1}}}_{4\text{-dim}} + \underbrace{\text{KL}_{\text{intra2}}}_{9\text{-dim}} + \underbrace{\text{KL}_{\text{cr1}\rightarrow 2}}_{6\text{-dim}} + \underbrace{\text{KL}_{\text{cr2}\rightarrow 1}}_{6\text{-dim}},$$

yielding four independently weighted penalty terms—one per group block. This is the mechanism that enables heterogeneous pruning allocation: setting  $\lambda_{\text{cross}} > \lambda_{\text{intra}}$  penalizes inter-group edges more heavily without affecting intra-group connectivity.

**Why this matters.** The block decomposition holds *because* the prior is block-diagonal—a flat isotropic prior  $\sigma_0^2 I$  does not factorize into group blocks (it mixes all edge dimensions equally), preventing independent per-group pruning control. The block-diagonal structure is the mathematical mechanism through which groups become the natural unit of edge pruning in HIBCG.

## H Worked Example: Group Priors and Block Decomposition with 10 Agents

This appendix section provides a fully worked numerical illustration for a concrete scenario with  $n = 10$  agents and two groups. We first demonstrate *why* the group-conditional prior is tighter than a flat prior (Proposition 4.2), then show *how* the block decomposition works (Proposition 4.3).

**Setup.** Consider 10 agents partitioned into  $g_1 = \{1, 2, 3, 4\}$  (4 agents) and  $g_2 = \{5, 6, 7, 8, 9, 10\}$  (6 agents). The full edge latent  $Z_A^{(l)} \in \mathbb{R}^{100}$  encodes the  $10 \times 10$  edge variables at layer  $l$ . We fix a single layer  $l$  and drop the superscript for clarity.

### Part I: Why the Group Prior is Tighter (Proposition 4.2)

**Modelling the true marginal.** Suppose the true aggregate posterior  $\bar{\mathbb{P}}(Z_A)$  is a Gaussian with block-correlated structure reflecting the groups:

$$\bar{\mathbb{P}}(Z_A) = \mathcal{N}(0, \bar{\Sigma}), \quad \bar{\Sigma} = \begin{pmatrix} \bar{\Sigma}_{\text{intra1}} & 0 & 0 & 0 \\ 0 & \bar{\Sigma}_{\text{intra2}} & 0 & 0 \\ 0 & 0 & \bar{\Sigma}_{\text{cross12}} & 0 \\ 0 & 0 & 0 & \bar{\Sigma}_{\text{cross21}} \end{pmatrix}, \quad (48)$$

where  $\bar{\Sigma}_{\text{intra1}} \in \mathbb{R}^{16 \times 16}$ ,  $\bar{\Sigma}_{\text{intra2}} \in \mathbb{R}^{36 \times 36}$ , and each cross block is  $24 \times 24$ . The block-diagonal structure encodes the fact that intra-group edge latents are correlated among themselves but approximately independent of cross-group latents.

For a concrete numerical instance, let each block be isotropic:  $\bar{\Sigma}_{\text{intra1}} = 0.9 I_{16}$ ,  $\bar{\Sigma}_{\text{intra2}} = 0.8 I_{36}$ ,  $\bar{\Sigma}_{\text{cross12}} = \bar{\Sigma}_{\text{cross21}} = 0.3 I_{24}$ .

#### Two priors.

- **Flat:**  $\mathbb{Q}_{\text{flat}} = \mathcal{N}(0, \sigma_0^2 I_{100})$  with  $\sigma_0^2 = 0.6$  (a single scale for all 100 dimensions).
- **Group:**  $\mathbb{Q}_{\text{group}} = \mathcal{N}(0, \text{blkdiag}(0.9 I_{16}, 0.8 I_{36}, 0.3 I_{24}, 0.3 I_{24}))$  (scales matched to the block variances of  $\bar{\mathbb{P}}$ ).

**Computing the prior mismatch KL.** For two zero-mean Gaussians in  $k$  dimensions with covariances  $\bar{\Sigma}$  and  $\Sigma_0$ :  $\text{KL}(\bar{\mathbb{P}} \| \mathbb{Q}) = \frac{1}{2}(\text{tr}(\Sigma_0^{-1} \bar{\Sigma}) - k + \ln |\Sigma_0| - \ln |\bar{\Sigma}|)$ . For isotropic blocks this simplifies to per-dimension terms:  $\text{KL}_{\text{block}} = \frac{k}{2}(\bar{\sigma}^2 / \sigma_0^2 - 1 + \ln(\sigma_0^2 / \bar{\sigma}^2))$ .

**Flat prior** ( $\sigma_0^2 = 0.6$  for all):

$$\begin{aligned} \text{intra-}g_1 &: \frac{16}{2}(0.9/0.6 - 1 + \ln(0.6/0.9)) = 8(1.5 - 1 - 0.405) = 8 \times 0.095 = 0.76, \\ \text{intra-}g_2 &: \frac{36}{2}(0.8/0.6 - 1 + \ln(0.6/0.8)) = 18(1.333 - 1 - 0.288) = 18 \times 0.046 = 0.82, \\ \text{cross (each)} &: \frac{24}{2}(0.3/0.6 - 1 + \ln(0.6/0.3)) = 12(0.5 - 1 + 0.693) = 12 \times 0.193 = 2.32. \end{aligned}$$

Total:  $\text{KL}(\bar{\mathbb{P}} \parallel \mathbb{Q}_{\text{flat}}) = 0.76 + 0.82 + 2.32 + 2.32 = \mathbf{6.22}$  nats.

**Group prior** (scales matched to blocks):

$$\begin{aligned} \text{intra-}g_1 &: \frac{16}{2}(0.9/0.9 - 1 + \ln(0.9/0.9)) = 8(1 - 1 + 0) = \mathbf{0}, \\ \text{intra-}g_2 &: \frac{36}{2}(0.8/0.8 - 1 + \ln(0.8/0.8)) = 18(1 - 1 + 0) = \mathbf{0}, \\ \text{cross (each)} &: \frac{24}{2}(0.3/0.3 - 1 + \ln(0.3/0.3)) = 12(1 - 1 + 0) = \mathbf{0}. \end{aligned}$$

Total:  $\text{KL}(\bar{\mathbb{P}} \parallel \mathbb{Q}_{\text{group}}) = \mathbf{0}$  nats.

**Tightness gap.** The gap from Proposition 4.2 is:

$$\text{KL}(\bar{\mathbb{P}} \parallel \mathbb{Q}_{\text{flat}}) - \text{KL}(\bar{\mathbb{P}} \parallel \mathbb{Q}_{\text{group}}) = 6.22 - 0 = \mathbf{6.22}$$
 nats.

In this idealized case (where we know the true marginal exactly), the group prior eliminates the mismatch entirely. In practice the group-conditional prior cannot match  $\bar{\mathbb{P}}$  perfectly, but it still captures the dominant block structure and substantially reduces the gap.

Even with a sub-optimal group prior—say  $\mathbb{Q}'_{\text{group}}$  with intra-block scale 0.7 and cross-block scale 0.4—the mismatch would be:

$$\begin{aligned} \text{intra-}g_1 &: 8(0.9/0.7 - 1 + \ln(0.7/0.9)) = 8(1.286 - 1 - 0.251) = 0.28, \\ \text{intra-}g_2 &: 18(0.8/0.7 - 1 + \ln(0.7/0.8)) = 18(1.143 - 1 - 0.134) = 0.16, \\ \text{cross (each)} &: 12(0.3/0.4 - 1 + \ln(0.4/0.3)) = 12(0.75 - 1 + 0.288) = 0.46. \end{aligned}$$

Total:  $\text{KL}(\bar{\mathbb{P}} \parallel \mathbb{Q}'_{\text{group}}) = 0.28 + 0.16 + 0.46 + 0.46 = \mathbf{1.36}$  nats, still a 78% reduction from the flat prior’s 6.22 nats.

**Key takeaway.** The group prior does not need to be perfectly matched to yield a substantial improvement. As long as the block structure is approximately correct, the variational bound is significantly tighter than with a flat prior—providing a concrete mathematical payoff for HIBCG’s group-conditional prior design (Definition 4.2).

## Part II: Block Decomposition (Proposition 4.3)

**Step 1: Partition edges into group blocks.** The group partition induces four blocks on the edge matrix:

$$\begin{aligned} B_{\text{intra1}} &= g_1 \times g_1 = \{(i, j) : i, j \in \{1, \dots, 4\}\}, & k_{\text{intra1}} &= 16, \\ B_{\text{intra2}} &= g_2 \times g_2 = \{(i, j) : i, j \in \{5, \dots, 10\}\}, & k_{\text{intra2}} &= 36, \\ B_{\text{cross12}} &= g_1 \times g_2 = \{(i, j) : i \in g_1, j \in g_2\}, & k_{\text{cross12}} &= 24, \\ B_{\text{cross21}} &= g_2 \times g_1 = \{(i, j) : i \in g_2, j \in g_1\}, & k_{\text{cross21}} &= 24. \end{aligned}$$

Note  $16 + 36 + 24 + 24 = 100$ , so all edge variables are covered.

**Step 2: Construct the block-diagonal prior.** Using isotropic blocks with different scales for intra- and cross-group edges:

$$\mathbb{Q}(Z_A) = \mathcal{N}\left(0, \text{blkdiag}(\sigma_{\text{intra}}^2 I_{16}, \sigma_{\text{intra}}^2 I_{36}, \sigma_{\text{cross}}^2 I_{24}, \sigma_{\text{cross}}^2 I_{24})\right). \quad (49)$$

This prior encodes the design choice that intra-group edges and cross-group edges may have different baseline “widths”. For instance, setting  $\sigma_{\text{intra}}^2 > \sigma_{\text{cross}}^2$  means the prior *expects* more variation within groups (denser connectivity) than across groups (sparser links).

**Step 3: Encoder parameterization.** The encoder produces per-block Gaussians. Suppose for one data point  $\mathcal{D}$ :

$$\begin{aligned}\mathbb{P}(Z_{A,\text{intra}1} \mid \mathcal{D}) &= \mathcal{N}(\mu_{\text{intra}1}, \text{diag}(\sigma_{\text{intra}1}^2)), & \mu_{\text{intra}1} &\in \mathbb{R}^{16}, \\ \mathbb{P}(Z_{A,\text{intra}2} \mid \mathcal{D}) &= \mathcal{N}(\mu_{\text{intra}2}, \text{diag}(\sigma_{\text{intra}2}^2)), & \mu_{\text{intra}2} &\in \mathbb{R}^{36}, \\ \mathbb{P}(Z_{A,\text{cross}12} \mid \mathcal{D}) &= \mathcal{N}(\mu_{\text{cross}12}, \text{diag}(\sigma_{\text{cross}12}^2)), & \mu_{\text{cross}12} &\in \mathbb{R}^{24}, \\ \mathbb{P}(Z_{A,\text{cross}21} \mid \mathcal{D}) &= \mathcal{N}(\mu_{\text{cross}21}, \text{diag}(\sigma_{\text{cross}21}^2)), & \mu_{\text{cross}21} &\in \mathbb{R}^{24}.\end{aligned}$$

**Step 4: Compute per-block KL divergences.** Applying Eq. (17) to each block:

$$\text{AIB}_{\text{intra}1} = \frac{1}{2} \sum_{d=1}^{16} \left( \frac{(\sigma_{\text{intra}1,d})^2 + (\mu_{\text{intra}1,d})^2}{\sigma_{\text{intra}}^2} - 1 + \log \frac{\sigma_{\text{intra}}^2}{(\sigma_{\text{intra}1,d})^2} \right), \quad (50)$$

and analogously for  $\text{AIB}_{\text{intra}2}$  (36 terms),  $\text{AIB}_{\text{cross}12}$  (24 terms, denominator  $\sigma_{\text{cross}}^2$ ), and  $\text{AIB}_{\text{cross}21}$  (24 terms). By Proposition 4.3:

$$\text{AIB}^{(l)} = \text{AIB}_{\text{intra}1} + \text{AIB}_{\text{intra}2} + \text{AIB}_{\text{cross}12} + \text{AIB}_{\text{cross}21}.$$

**Step 5: Apply heterogeneous pruning weights.** The structural penalty becomes:

$$\mathcal{L}_{\text{AIB}}^{(l)} = \lambda_{\text{intra}} \cdot (\text{AIB}_{\text{intra}1} + \text{AIB}_{\text{intra}2}) + \lambda_{\text{cross}} \cdot (\text{AIB}_{\text{cross}12} + \text{AIB}_{\text{cross}21}). \quad (51)$$

Setting  $\lambda_{\text{cross}} > \lambda_{\text{intra}}$  encourages the model to prune cross-group edges more aggressively than intra-group edges.

**Numerical illustration.** As a concrete instance, suppose  $\sigma_{\text{intra}}^2 = 1.0$ ,  $\sigma_{\text{cross}}^2 = 0.5$ , and the encoder outputs (averaged over a minibatch) have intra-block means  $\bar{\mu} \approx 0.3$ ,  $\bar{\sigma}^2 \approx 0.8$  and cross-block means  $\bar{\mu} \approx 0.1$ ,  $\bar{\sigma}^2 \approx 0.3$ . Then the per-dimension KL is approximately:

$$\begin{aligned}\text{intra: } & \frac{1}{2}(0.8/1.0 + 0.09/1.0 - 1 + \ln(1.0/0.8)) \approx \frac{1}{2}(0.8 + 0.09 - 1 + 0.223) \approx 0.057, \\ \text{cross: } & \frac{1}{2}(0.3/0.5 + 0.01/0.5 - 1 + \ln(0.5/0.3)) \approx \frac{1}{2}(0.6 + 0.02 - 1 + 0.511) \approx 0.066.\end{aligned}$$

Multiplying by block dimension gives:  $\text{AIB}_{\text{intra}1} \approx 16 \times 0.057 = 0.91$ ,  $\text{AIB}_{\text{intra}2} \approx 36 \times 0.057 = 2.05$ ,  $\text{AIB}_{\text{cross}12} \approx 24 \times 0.066 = 1.58$ ,  $\text{AIB}_{\text{cross}21} \approx 24 \times 0.066 = 1.58$ . Total:  $\text{AIB}^{(l)} \approx 6.12$  nats.

With  $\lambda_{\text{intra}} = 0.001$  and  $\lambda_{\text{cross}} = 0.01$ , the penalty contribution is  $0.001 \times (0.91 + 2.05) + 0.01 \times (1.58 + 1.58) = 0.003 + 0.032 = 0.035$ , where over 90% of the penalty comes from cross-group edges despite them contributing only about half the total KL. This asymmetric penalization drives cross-group sparsity while preserving intra-group density—exactly the behavior described in Section 4.1.

**Contrast with a flat prior.** Under a flat prior  $\mathcal{N}(0, \sigma_0^2 I_{100})$ , all 100 edge latents share the same prior variance and penalty weight. It is impossible to impose  $\lambda_{\text{cross}} > \lambda_{\text{intra}}$  because the KL does not decompose into group blocks—the prior mixes all dimensions equally. This is the fundamental limitation that HIBCG’s group-aware design overcomes.

## I Proof of Relevance via Q-Value Optimization (Proposition 4.4)

**Proposition** (4.4, Relevance via Q-Value Optimization). *Let  $Y = (a_1^*, \dots, a_n^*)$  denote the optimal joint action and  $K = \prod_i |\mathcal{U}_i|$  the joint action-space size. Assume:*

- (A1) *QMIX-style monotonic value decomposition with greedy action selection  $a_i = \arg \max_{u_i} Q_i(\tau_i, u_i, Z_{X,i}^{(L)})$ ;*
- (A2) *the target network has converged, so that  $\mathcal{L}_{\text{TD}} = \mathbb{E}[e^2]$  with  $e(s, \mathbf{u}) = Q_{\text{tot}}(s, \mathbf{u}) - Q^*(s, \mathbf{u})$ ;*
- (A3) *the minimum action-value gap  $\Delta_{\min} \triangleq \min_s \min_{\mathbf{u} \neq Y} (Q^*(s, Y) - Q^*(s, \mathbf{u})) > 0$  (i.e., the optimal joint action is unique for every state).*

Under (A1)–(A3), the TD loss  $\mathcal{L}_{\text{TD}}$  serves as a surrogate for maximizing the relevance term  $I(Y; Z_X^{(L)})$  in the IB objective (2). Specifically:

$$I(Y; Z_X^{(L)}) \geq H(Y) - h\left(\frac{\mathcal{L}_{\text{TD}}}{c}\right) - \frac{\mathcal{L}_{\text{TD}}}{c} \log(K-1),$$

where  $h(p) = -p \log p - (1-p) \log(1-p)$  is the binary entropy and  $c \triangleq \Delta_{\min}^2 / (4K) > 0$ . The bound is valid when  $\mathcal{L}_{\text{TD}}/c \leq \frac{K-1}{K}$ ; for larger errors, the bound is vacuously true. Since both the second term  $h(\mathcal{L}_{\text{TD}}/c)$  and the third term  $(\mathcal{L}_{\text{TD}}/c) \log(K-1)$  vanish as  $\mathcal{L}_{\text{TD}} \rightarrow 0$ , minimizing  $\mathcal{L}_{\text{TD}}$  tightens the lower bound towards  $H(Y)$ , ensuring  $Z_X^{(L)}$  preserves task-relevant information.

*Proof.* We proceed in five steps, organized into three logical parts: (i) algebraic analysis showing that small approximation errors preserve the ordering of Q-values (Steps 1–2); (ii) Markov’s inequality to translate the mean-squared TD loss into a bound on the action prediction error  $P_e$  (Step 3); (iii) Fano’s inequality and DPI to convert the  $P_e$  bound into the desired lower bound on  $I(Y; Z_X^{(L)})$  (Steps 4–5).

**Step 1: Define the quantities.** Let  $Y = (a_1^*, \dots, a_n^*)$  denote the optimal joint action under the true Q-function, and let  $Z_X^{(L)}$  denote the final-layer node representations from which individual Q-values are computed via  $Q_i(\tau_i, u_i) = f_i(Z_{X,i}^{(L)}, u_i)$ . Under QMIX-style monotonic mixing, the joint Q-value is  $Q_{\text{tot}} = \text{mix}(Q_1, \dots, Q_n; s)$  with  $\partial Q_{\text{tot}} / \partial Q_i \geq 0$ .

**Step 2: Q-value separation under approximation error.** The TD loss is

$$\mathcal{L}_{\text{TD}} = \mathbb{E}_{(s, \mathbf{u}, r, s') \sim \mathcal{D}} [(Q_{\text{tot}}(s, \mathbf{u}; \theta) - y_{\text{target}})^2], \quad y_{\text{target}} = r + \gamma \max_{\mathbf{u}'} Q'_{\text{tot}}(s', \mathbf{u}'; \theta^-). \quad (52)$$

For a given state  $s$  and joint action  $\mathbf{u}$ , define the approximation error

$$e(s, \mathbf{u}) \triangleq Q_{\text{tot}}(s, \mathbf{u}) - Q^*(s, \mathbf{u}), \quad (53)$$

so that  $\mathcal{L}_{\text{TD}} = \mathbb{E}[e(s, \mathbf{u})^2]$  by assumption (A2) (target network convergence:  $y_{\text{target}} \approx Q^*$ ). For any pair of joint actions  $\mathbf{u} \neq \mathbf{u}'$ , the learned Q-gap decomposes as

$$Q_{\text{tot}}(s, \mathbf{u}) - Q_{\text{tot}}(s, \mathbf{u}') = \underbrace{(Q^*(s, \mathbf{u}) - Q^*(s, \mathbf{u}'))}_{\text{true gap}} + \underbrace{(e(s, \mathbf{u}) - e(s, \mathbf{u}'))}_{\text{error difference}}. \quad (54)$$

Taking absolute values on both sides of (54) and applying the reverse triangle inequality:

$$\begin{aligned} \underbrace{|Q_{\text{tot}}(s, \mathbf{u}) - Q_{\text{tot}}(s, \mathbf{u}')|}_{\text{learned gap}} &= |(Q^*(s, \mathbf{u}) - Q^*(s, \mathbf{u}')) + (e(s, \mathbf{u}) - e(s, \mathbf{u}'))| \\ &\geq \underbrace{|Q^*(s, \mathbf{u}) - Q^*(s, \mathbf{u}')|}_{\text{true gap}} - \underbrace{|e(s, \mathbf{u}) - e(s, \mathbf{u}')|}_{\text{error difference}}. \end{aligned} \quad (55)$$

This is a *worst-case guarantee*: the learned gap can never be smaller than the true gap minus the error difference. In reinforcement learning, correct action selection depends only on *ranking*—as long as the learned gap stays strictly positive, the greedy policy selects the optimal action. Conversely, if the error difference exceeds the true gap, the right-hand side becomes negative and the network may pick a wrong action. The triangle inequality further bounds the error difference by  $|e(s, \mathbf{u}) - e(s, \mathbf{u}')| \leq |e(s, \mathbf{u})| + |e(s, \mathbf{u}')|$ , so controlling individual approximation errors suffices to preserve the correct ranking. The next step makes this precise by quantifying *how small* the errors must be to guarantee correct action selection.

**Step 3: From Q-accuracy to action prediction.** We now connect the approximation error to the probability of selecting a wrong action. Define the *action prediction error*

$$P_e = \Pr[\arg \max_{\mathbf{u}} Q_{\text{tot}}(s, \mathbf{u}; \theta) \neq Y], \quad (56)$$

and the *minimum action-value gap* (assumption (A3)):

$$\Delta_{\min} = \min_s \min_{\mathbf{u} \neq Y} (Q^*(s, Y) - Q^*(s, \mathbf{u})) > 0, \quad (57)$$

which measures the smallest margin by which the optimal joint action  $Y$  outperforms any suboptimal alternative under  $Q^*$ . The strict positivity of  $\Delta_{\min}$  is guaranteed by assumption (A3) and is necessary for the Markov-inequality step below. We also write the state-specific gap  $\Delta(s) \triangleq \min_{\mathbf{u} \neq Y} (Q^*(s, Y) - Q^*(s, \mathbf{u})) \geq \Delta_{\min}$ .

**Exact recovery regime** ( $P_e = 0$ ). We argue by contradiction. For a prediction error at state  $s$ , there must exist some  $\mathbf{u}' \neq Y$  with  $Q_{\text{tot}}(s, \mathbf{u}') \geq Q_{\text{tot}}(s, Y)$ , i.e., the learned  $Q$ -values rank a suboptimal action at least as high as the optimal one. Setting  $\mathbf{u} = Y$  in (55) and noting  $Q^*(s, Y) - Q^*(s, \mathbf{u}') \geq \Delta(s) \geq \Delta_{\min}$ :

$$\underbrace{Q_{\text{tot}}(s, Y) - Q_{\text{tot}}(s, \mathbf{u}')}_{\leq 0 \text{ if error occurs}} \geq \Delta(s) - |e(s, Y)| - |e(s, \mathbf{u}')|. \quad (58)$$

If an error occurs, the left-hand side is  $\leq 0$ , forcing the right-hand side to be  $\leq 0$  as well. Rearranging:

$$\Delta_{\min} \leq \Delta(s) \leq |e(s, Y)| + |e(s, \mathbf{u}')|. \quad (59)$$

That is, *making a mistake requires the sum of the two approximation errors to reach at least  $\Delta_{\min}$* . If every error satisfies  $|e(s, \mathbf{u})| < \Delta_{\min}/2$ , then  $|e(s, Y)| + |e(s, \mathbf{u}')| < \Delta_{\min}$ , contradicting (59). Hence no error can occur and  $P_e = 0$ .

**General bound via Markov's inequality.** More generally, for a prediction error at state  $s$  the learned gap  $Q_{\text{tot}}(s, Y) - Q_{\text{tot}}(s, \mathbf{u}')$  must be non-positive for some  $\mathbf{u}' \neq Y$ . Chaining this with (58):

$$0 \geq Q_{\text{tot}}(s, Y) - Q_{\text{tot}}(s, \mathbf{u}') \geq \Delta(s) - |e(s, Y)| - |e(s, \mathbf{u}')|, \quad (60)$$

which rearranges to  $|e(s, Y)| + |e(s, \mathbf{u}')| \geq \Delta(s) \geq \Delta_{\min}$ . Since the sum of two non-negative numbers exceeds  $\Delta_{\min}$ , at least one of them must exceed  $\Delta_{\min}/2$ , i.e.,  $|e(s, \mathbf{u})| \geq \Delta_{\min}/2$  for at least one action  $\mathbf{u}$ . We square both sides to obtain  $e(s, \mathbf{u})^2 \geq \Delta_{\min}^2/4$ —this reformulation in terms of squared errors is deliberate: the TD loss is defined as  $\mathcal{L}_{\text{TD}} = \mathbb{E}[e(s, \mathbf{u})^2]$  (assumption (A2)), so the squared form lets us apply Markov's inequality directly with  $X = e^2$  and  $\mathbb{E}[X] = \mathcal{L}_{\text{TD}}$ .

**State-level error and Markov's inequality.** Define the average squared error at state  $s$ :

$$\bar{E}(s) \triangleq \frac{1}{K} \sum_{\mathbf{u}} e(s, \mathbf{u})^2. \quad (61)$$

For any state  $s$  where the greedy action is wrong, at least one action  $\mathbf{u}^*$  satisfies  $e(s, \mathbf{u}^*)^2 \geq \Delta_{\min}^2/4$ , and therefore  $\bar{E}(s) \geq \Delta_{\min}^2/(4K)$ . Applying *Markov's inequality* ( $\Pr[X \geq a] \leq \mathbb{E}[X]/a$  for non-negative  $X$ ) to  $X = \bar{E}(s)$  with  $a = \Delta_{\min}^2/(4K)$ :

$$P_e \leq \Pr_s \left[ \bar{E}(s) \geq \frac{\Delta_{\min}^2}{4K} \right] \leq \frac{\mathbb{E}_s[\bar{E}(s)]}{\Delta_{\min}^2/(4K)} = \frac{\mathcal{L}_{\text{TD}}}{\Delta_{\min}^2/(4K)}, \quad (62)$$

where the last equality uses  $\mathbb{E}_s[\bar{E}(s)] = \mathbb{E}_{(s, \mathbf{u})}[e(s, \mathbf{u})^2] = \mathcal{L}_{\text{TD}}$  (here we assume the replay distribution has uniform coverage over actions for each state, so that the uniform average in  $\bar{E}(s)$  matches the expectation under  $\mathcal{D}$ ; this is satisfied, e.g., when the replay buffer is large and the behavior policy is sufficiently exploratory). Setting  $c \triangleq \Delta_{\min}^2/(4K) > 0$ :

$$P_e \leq \frac{\mathcal{L}_{\text{TD}}}{c}. \quad (63)$$

The factor of  $K$  reflects a fundamental vulnerability of greedy action selection: the policy fails if even one out of  $K$  joint actions has a large overestimation error. Because the TD loss  $\mathcal{L}_{\text{TD}}$  averages over the entire state-action distribution, a single fatal error gets diluted by a factor of  $1/K$ . Therefore, to guarantee that the worst-case individual action error remains below the safe threshold, the average TD loss must be bounded proportionally tighter by a factor of  $K$ .

**Step 4: Apply Fano’s inequality and DPI.** We now translate the prediction-error bound into an information-theoretic statement in two sub-steps.

*Sub-step 4a: Fano’s inequality.* For any random variable  $Y$  taking values in  $\mathcal{Y}$  with  $|\mathcal{Y}| = K$  and any estimator  $\hat{Y}$  with error probability  $P_e = \Pr[\hat{Y} \neq Y]$ , the standard **Fano’s inequality** [57] upper-bounds the residual uncertainty of  $Y$  given the prediction  $\hat{Y}$ :

$$H(Y | \hat{Y}) \leq \underbrace{h(P_e)}_{\text{uncertainty from error occurrence}} + \underbrace{P_e \log(K-1)}_{\text{uncertainty over wrong outcomes}}, \quad (64)$$

where  $h(p) = -p \log p - (1-p) \log(1-p)$  is the binary entropy function. The first term captures the uncertainty of *whether* an error occurs; the second accounts for *which* of the  $K-1$  wrong outcomes is selected, given that an error occurs. For multi-agent action spaces,  $K = \prod_i |\mathcal{U}_i|$ .

*Sub-step 4b: Data Processing Inequality (DPI).* We must relate the prediction  $\hat{Y}$  back to the latent representation  $Z_X^{(L)}$ . In our architecture, the chosen action  $\hat{Y} = \arg \max_{\mathbf{u}} Q_{\text{tot}}(s, \mathbf{u})$  is a deterministic function of  $Z_X^{(L)}$ . The **DPI** guarantees that a deterministic post-processing cannot increase the information a variable carries about  $Y$ ; equivalently, conditioning on the richer representation  $Z_X^{(L)}$  leaves at most as much residual uncertainty as conditioning on  $\hat{Y}$ :

$$H(Y | Z_X^{(L)}) \leq H(Y | \hat{Y}). \quad (65)$$

Chaining (65) with Fano’s bound (64):

$$H(Y | Z_X^{(L)}) \leq h(P_e) + P_e \log(K-1). \quad (66)$$

**Step 5: Derive the mutual information bound.** The mutual information decomposes as  $I(Y; Z_X^{(L)}) = H(Y) - H(Y | Z_X^{(L)})$ . Substituting the Fano upper bound (66) for the conditional entropy and the prediction-error bound (63) for  $P_e$ :

$$\begin{aligned} I(Y; Z_X^{(L)}) &= H(Y) - H(Y | Z_X^{(L)}) \\ &\geq H(Y) - h(P_e) - P_e \log(K-1) && \text{(Fano + DPI, Eq. 66)} \\ &\geq H(Y) - h\left(\frac{\mathcal{L}_{\text{TD}}}{c}\right) - \frac{\mathcal{L}_{\text{TD}}}{c} \log(K-1). && \text{(Markov, Eq. 63)} \end{aligned} \quad (67)$$

Note that replacing  $P_e$  with its upper bound  $\mathcal{L}_{\text{TD}}/c$  in the final inequality is valid because the function  $f(p) = h(p) + p \log(K-1)$  is monotonically increasing for  $p \leq \frac{K-1}{K}$ . This is exactly the bound (10) stated in Proposition 4.4, completing the proof.  $\square$

**Interpretation.** The constant  $c = \Delta_{\min}^2/(4K)$  depends on the minimum action-value gap and the joint action-space size  $K$  of the environment—tasks with well-separated optimal actions (large  $\Delta_{\min}$ ) yield a tighter bound. Both  $h(\mathcal{L}_{\text{TD}}/c)$  and  $(\mathcal{L}_{\text{TD}}/c) \log(K-1)$  vanish as  $\mathcal{L}_{\text{TD}} \rightarrow 0$ , so the lower bound approaches the maximum value  $H(Y)$ . The key insight is that the TD loss *implicitly* maximizes the IB relevance term: by making  $Q_{\text{tot}}$  more accurate, it ensures the representations  $Z_X^{(L)}$  retain enough information to identify optimal actions. This justifies using  $\mathcal{L}_{\text{TD}}$  as the relevance surrogate in the HIBCG objective (13) without needing an explicit variational decoder for  $I(Y; Z_X^{(L)})$ .

**Remark: asymptotic scaling for small error.** Write  $p \triangleq \mathcal{L}_{\text{TD}}/c$  for brevity. When  $p \ll 1$ , we can expand the binary entropy: for small  $p$ ,  $-(1-p) \log(1-p) = p \log e + O(p^2)$ , which is  $O(p)$  and dominated by  $-p \log p = O(p \log(1/p))$ . Hence  $h(p) = -p \log p + O(p)$ , and substituting into (67) gives the asymptotic form

$$I(Y; Z_X^{(L)}) \geq H(Y) - \frac{\mathcal{L}_{\text{TD}}}{c} \log \frac{K-1}{\mathcal{L}_{\text{TD}}/c} + O\left(\frac{\mathcal{L}_{\text{TD}}}{c}\right), \quad (68)$$

confirming that the gap to  $H(Y)$  vanishes at a quasi-linear rate  $\Theta\left(\frac{\mathcal{L}_{\text{TD}}}{c} \log \frac{K-1}{\mathcal{L}_{\text{TD}}/c}\right)$ —slightly *slower* than linear in  $\mathcal{L}_{\text{TD}}$  because the logarithmic factor  $\log \frac{K-1}{\mathcal{L}_{\text{TD}}/c} \rightarrow \infty$  as  $\mathcal{L}_{\text{TD}} \rightarrow 0$ , yet still  $o(p^\alpha)$  for every  $\alpha < 1$ .

## J Proof of Optimal Compression Allocation: Water-Filling (Proposition 4.5)

**Proposition** (4.5, Optimal Compression Allocation: Water-Filling). *Consider the constrained optimization problem of minimizing the TD loss  $\min_{\theta} \mathcal{L}_{\text{TD}}(\theta)$  subject to a total information bottleneck capacity  $\sum_{l,g} \text{AIB}^{(l,g)} + \sum_{l,i} \text{XIB}^{(l,i)} \leq \mathcal{B}$ . At optimality, the Karush-Kuhn-Tucker (KKT) conditions require that the marginal utility of information is equalized across all active channels (i.e., channels where information is actually transmitted):*

$$-\frac{\partial \mathcal{L}_{\text{TD}}}{\partial \text{AIB}^{(l,g)}} = -\frac{\partial \mathcal{L}_{\text{TD}}}{\partial \text{XIB}^{(l',i)}} = \nu \quad \forall (l,g), (l',i) \text{ with active budgets,}$$

where  $\nu \geq 0$  is the global Lagrange multiplier (the “water level”).

*Proof.* We show that the KKT conditions of the constrained problem yield a water-filling allocation, leading to *heterogeneous* compression—the central property that distinguishes HIBCG from flat IB methods. The proof proceeds in six steps.

**Step 1: Formalize the constrained problem.** Recall that HIBCG uses two families of information bottleneck terms:  $\text{AIB}^{(l,g)}$  controls how many nats of graph structure (adjacency) are retained at layer  $l$  for group-block  $g$ , and  $\text{XIB}^{(l,i)}$  controls how many nats of node features (messages) agent  $i$  retains at layer  $l$ . To unify notation, let  $\mathcal{C} = \mathcal{C}_A \cup \mathcal{C}_X$  denote the full set of communication channels, where  $\mathcal{C}_A = \{(l,g)\}$  indexes AIB channels and  $\mathcal{C}_X = \{(l,i)\}$  indexes XIB channels. For each channel  $c \in \mathcal{C}$ , we write

$$R_c \triangleq \begin{cases} \text{AIB}^{(l,g)} & \text{if } c = (l,g) \in \mathcal{C}_A, \\ \text{XIB}^{(l,i)} & \text{if } c = (l,i) \in \mathcal{C}_X, \end{cases} \quad (69)$$

for its information rate.

In practice, these rates are determined by the neural network parameters  $\theta$ . However, for the theoretical purpose of deriving the optimal budget allocation, we adopt the standard information-theoretic *rate-distortion view* [57]. Instead of optimizing over the complex parameter space  $\theta$ , we treat the rates  $(R_c)_{c \in \mathcal{C}}$  directly as the decision variables. We define  $\mathcal{L}_{\text{TD}}(R_1, \dots, R_{|\mathcal{C}|})$  as the theoretically minimum achievable TD loss when the network is perfectly optimized under the constraint that each channel  $c$  carries exactly  $R_c$  nats. (We discuss the connection back to practical parameter-level optimization via the chain rule in the remark at the end of this proof.)

Using this abstraction, we formulate the global allocation task as a continuous constrained optimization problem over the rates:

$$\min_{\{R_c \geq 0\}} \mathcal{L}_{\text{TD}}(R_1, \dots, R_{|\mathcal{C}|}) \quad \text{subject to} \quad \sum_{c \in \mathcal{C}} R_c \leq \mathcal{B}. \quad (70)$$

**Step 2: Write the Lagrangian.** To solve (70) we use the **Karush–Kuhn–Tucker (KKT) conditions**, which generalize Lagrange multipliers to inequality constraints. Standard convention rewrites every constraint into the form  $g(\cdot) \leq 0$  and pairs it with a non-negative multiplier. We have two families:

1. **The budget constraint:**  $\sum_{c \in \mathcal{C}} R_c \leq \mathcal{B}$  becomes  $\sum_{c \in \mathcal{C}} R_c - \mathcal{B} \leq 0$ . We assign this a global multiplier  $\nu \geq 0$ .
2. **The non-negativity constraints:**  $R_c \geq 0$  becomes  $-R_c \leq 0$  for each channel. We assign individual multipliers  $\eta_c \geq 0$  to each.

Adding these constraint terms to the main objective  $\mathcal{L}_{\text{TD}}(\{R_c\})$ , we obtain the Lagrangian:

$$\mathfrak{L}(\{R_c\}, \nu, \{\eta_c\}) = \mathcal{L}_{\text{TD}}(\{R_c\}) + \nu \left( \sum_{c \in \mathcal{C}} R_c - \mathcal{B} \right) - \sum_{c \in \mathcal{C}} \eta_c R_c. \quad (71)$$

Intuitively,  $\nu$  represents the global “shadow price” of information: every additional nat of information allowed by the budget constraint reduces the objective penalty. Conversely, allocating a nat to any channel incurs a cost of  $\nu$  in the optimization.

**Step 3: Apply the KKT conditions.** At a local optimum  $\{R_c^*\}$ , the KKT necessary conditions hold. (The required constraint qualification—Slater’s condition—is satisfied because a strictly feasible point  $\sum_c R_c < \mathcal{B}$  exists: simply set all rates small enough.) These conditions are:

1. *Stationarity.* The gradient of the Lagrangian with respect to each rate  $R_c$  must be zero:

$$\frac{\partial \mathcal{L}_{\text{TD}}}{\partial R_c} + \nu - \eta_c = 0 \quad \forall c \in \mathcal{C}. \quad (72)$$

2. *Complementary slackness.* The product of a multiplier and its constraint must be zero:

$$\nu \left( \sum_{c \in \mathcal{C}} R_c^* - \mathcal{B} \right) = 0, \quad \text{and} \quad \eta_c R_c^* = 0 \quad \forall c \in \mathcal{C}. \quad (73)$$

This means: if a constraint is not “tight” (not hitting the boundary), its multiplier must be zero. In particular, if a channel is transmitting information ( $R_c^* > 0$ ), then its non-negativity multiplier must vanish ( $\eta_c = 0$ ).

3. *Dual feasibility.* The multipliers cannot be negative:  $\nu \geq 0$  and  $\eta_c \geq 0$  for all  $c$ .

**Step 4: Isolate the marginal utility.** To understand the physical meaning of the KKT conditions, we first rearrange the stationarity condition (Eq. (72) from Step 3) to isolate the gradient of the objective function:

$$-\frac{\partial \mathcal{L}_{\text{TD}}}{\partial R_c} = \nu - \eta_c. \quad (74)$$

The left-hand side of this equation represents a crucial quantity in resource allocation: the *marginal utility* of channel  $c$ . It directly answers the question: how much does the task performance improve (i.e., how much does the TD loss decrease) if we allow one additional nat of information through that specific channel?

Formally, we define this marginal utility, evaluated at the optimal allocation  $R^*$ , as:

$$U_c \triangleq -\left. \frac{\partial \mathcal{L}_{\text{TD}}}{\partial R_c} \right|_{R=R^*} \geq 0. \quad (75)$$

In other words,  $U_c$  quantifies how much the TD loss shrinks per additional nat of information allocated to channel  $c$ . The non-negativity  $U_c \geq 0$  follows directly from rate-distortion monotonicity: an encoder can always ignore extra capacity to replicate a lower-rate policy, guaranteeing that more information never degrades performance. Consequently, a large  $U_c$  identifies a communication *bottleneck* where extra capacity drastically improves coordination, whereas a small  $U_c$  indicates the channel carries mostly *redundant* or task-irrelevant information. We now show how Eq. (74) forces the optimal allocation to equalize  $U_c$  across all active channels—the defining property of water-filling.

**Step 5: Derive the water-filling condition.** Substituting the definition of marginal utility into the stationarity condition yields  $U_c = \nu - \eta_c$ . We distinguish two cases based on the allocation  $R_c^*$ :

**Case A: Active channel** ( $R_c^* > 0$ ). By complementary slackness ( $\eta_c R_c^* = 0$ ), the penalty multiplier must be  $\eta_c = 0$ , which forces:

$$U_c = \nu. \quad (76)$$

This reveals that all active channels share the *exact same* marginal utility, equalizing at the global multiplier  $\nu$ . This equilibrium relies on the standard information-theoretic assumption of diminishing returns (convexity of the rate-distortion function): as more rate is allocated to a channel, its marginal utility decreases. If one active channel temporarily had  $U_c > \nu$ , the optimizer would shift more budget towards it. This influx of capacity would drive its marginal utility down until it perfectly aligned with the global water level  $\nu$ .

**Case B: Inactive channel** ( $R_c^* = 0$ ). If no information is allocated, the non-negativity multiplier  $\eta_c \geq 0$  is unconstrained. Thus:

$$U_c = \nu - \eta_c \leq \nu. \quad (77)$$

Inactive channels have a marginal utility *at or below* the water level. Even at zero allocated rate, their potential contribution is so low that any allocation would not justify the cost  $\nu$ .

**Step 6: Summary of the water-filling principle.** Combining Cases A and B, the optimal allocation strictly adheres to a thresholding rule:

$$R_c^* \text{ is } \begin{cases} > 0 & \text{if } U_c = \nu \quad (\text{channel is active}), \\ = 0 & \text{if } U_c < \nu \quad (\text{channel is shut off}). \end{cases} \quad (78)$$

To understand this physically, imagine the budget  $\mathcal{B}$  as a limited volume of water. If the neural network is starved for information (i.e., it wants to use more than  $\mathcal{B}$  to minimize the TD loss), information becomes a scarce and valuable resource. In this scenario, the optimization will spend every last drop of the budget ( $\sum_c R_c^* = \mathcal{B}$ ), which creates a strictly positive “price” for information ( $\nu > 0$ ).

This allocation perfectly mirrors the classical **water-filling algorithm** [57], governed by gravity and diminishing returns:

1. **Pouring:** The optimization “pours” the budget into the communication channels, naturally prioritizing those with the deepest need (the highest initial marginal utility  $U_c$ ).
2. **Spilling over:** As a channel fills with information, its utility drops. The water naturally spills over into the next most useful channels to maintain equilibrium.
3. **Settling:** When the budget is completely exhausted, the marginal utilities of all active channels form a perfectly flat surface exactly at level  $\nu$ .

Any channel whose potential utility is worse than this final water level ( $U_c < \nu$ ) remains completely dry ( $R_c^* = 0$ ). Conversely, if the budget  $\mathcal{B}$  is so large that the network does not even need it all, information is effectively free ( $\nu = 0$ ), and no channel is restricted.

**Connection to the proposition statement.** Recalling from Step 1 that  $R_c$  is either  $\text{AIB}^{(l,g)}$  or  $\text{XIB}^{(l,i)}$ , Case A directly translates  $U_c = \nu$  back into the channel-specific form stated in Proposition 4.5:

$$-\frac{\partial \mathcal{L}_{\text{TD}}}{\partial \text{AIB}^{(l,g)}} = -\frac{\partial \mathcal{L}_{\text{TD}}}{\partial \text{XIB}^{(l',i)}} = \nu \quad \forall (l,g), (l',i) \text{ with } R_c^* > 0.$$

That is, the marginal utility of every active AIB channel equals that of every active XIB channel, all locked at the common water level  $\nu$ . This completes the proof of Proposition 4.5.  $\square$

**Remark: From rate space to parameter space.** The proof above adopts the information-theoretic *rate-distortion view*, treating the channel capacities ( $R_c$ ) as direct decision variables. In practice, our HI-BCG architecture optimizes neural network parameters  $\theta$ , and the rates  $R_c(\theta)$  are explicitly parameterized by  $\theta$ . The theoretical water-filling conditions derived in rate space are mathematically inherited by the parameter-level problem under standard constraint qualifications (e.g., the Linear Independence Constraint Qualification). Specifically, if the Jacobian matrix of the rates with respect to the parameters,  $\nabla_{\theta} \mathbf{R}(\theta)$ , has full row rank at the optimum  $\theta^*$ , then the parameter-level gradients can independently control each channel’s rate, preserving the exact water-filling structure. In our GNN architecture, each information-bottleneck channel has dedicated variational parameters (e.g., per-edge sampling logits for the AIB, and per-node encoder weights for the XIB). This architectural decoupling ensures the full-rank Jacobian condition is easily satisfied in practice, making our theoretical water-filling framework a highly accurate model of the network’s actual training dynamics.

**Heterogeneous allocation in HIBCG.** The most important consequence of the water-filling principle is that it produces *heterogeneous* compression: HIBCG does not prune edges or compress messages uniformly, but directs every bit of retained capacity to the most task-critical coordination links. Concretely, the KKT conditions dictate that:

- **High-utility channels receive more bits.** Intra-group AIB channels ( $\text{AIB}^{(l,g_a \times g_a)}$ ) and XIB channels of boundary agents (who carry unique observations) have large  $U_c$ , so they are “above the water level” and receive generous rates  $R_c$ . This preserves the dense intra-group coordination that cooperative tasks require.

- **Low-utility channels are compressed or shut off.** Cross-group AIB channels ( $\text{AIB}^{(l,g_a \times g_b)}$ ) and XIB channels of agents deep inside homogeneous groups have small  $U_c$ , placing them “below the water level.” These channels are aggressively compressed or eliminated, producing the sparse inter-group topology observed in our experiments.

This principled, utility-driven allocation is what distinguishes HIBCG from flat IB methods that apply a single global  $\beta$  to all channels indiscriminately: the water-filling structure guarantees that the limited information capacity is spent where it matters most for task performance.

**Connection to the penalty-form objective.** In practice, HIBCG uses the unconstrained penalty form

$$\mathcal{L} = \mathcal{L}_{\text{TD}} + \sum_{(l,g) \in \mathcal{C}_A} \lambda_{l,g}^A \text{AIB}^{(l,g)} + \sum_{(l,i) \in \mathcal{C}_X} \lambda_{l,i}^X \text{XIB}^{(l,i)}. \quad (79)$$

Comparing with the Lagrangian (71), the fixed penalty weights  $\lambda_c$  play the role of  $\nu - \eta_c$ . When the penalty weights are chosen proportional to dimensionality ( $\lambda_c = \lambda_{\text{dim}} \cdot \text{dim}(c)$ ), the model converges to a *local* water-filling solution where channels of the same type and dimensionality are equalized. Adaptive dual-ascent schedules (Section K below) more closely track the true water-filling optimum by adjusting  $\lambda_c$  towards the global water level  $\nu$ .

## K Dual-Ascent Variant for Adaptive Capacity Control

The penalty-form objective in Eq. (19) requires the user to fix per-block multipliers  $\lambda_A^{(l,g)}$ . As an alternative, HIBCG admits a constrained dual-ascent formulation that automatically drives  $\lambda_A^{(l,g)}$  toward the water-filling level  $\nu$  of Proposition 4.5, without manual tuning. Replace the penalty form by:

$$\begin{aligned} \mathcal{L} &= \mathcal{L}_{\text{task}} + \sum_{l,g} \lambda_A^{(l,g)} \left( \widehat{\text{AIB}}^{(l,g)} - C_A^{(l,g)} \right), \\ \lambda_A^{(l,g)} &\leftarrow \left[ \lambda_A^{(l,g)} + \eta_A \left( \widehat{\text{AIB}}^{(l,g)} - C_A^{(l,g)} \right) \right]_+, \end{aligned} \quad (80)$$

with per-block rate targets  $C_A^{(l,g)} = c_A \cdot k_{l,g}$  and dual learning rate  $\eta_A$ . Because the projection onto  $[0, \infty)$  is exact and the inner minimisation is differentiable,  $\lambda_A^{(l,g)}$  converges to a stationary point of the Lagrangian; under the standard constraint qualifications discussed above, this stationary point coincides with the global water level  $\nu$ . The XIB multipliers admit an identical update with rates  $C_X^{(l,i)} = c_X \cdot d_L$ . In our experiments the fixed-penalty form is sufficient (HIBCG already attains a  $906\times$  cross/intra ratio without dual ascent), so we use it throughout for simplicity.

## L Implementation Details and Training Algorithm

HIBCG is built on the EPyMARL framework. All configurations use a GRU-based agent network with hidden dimension 64 (128 for MAgent),  $\epsilon$ -greedy exploration annealed over 50k–1M steps (environment-dependent), target network updated every 200 steps, and a replay buffer of size 5000 (1000 for MAgent). The GCN message dimension is  $0.3 \times d_{\text{obs}}$  for SMACv1 and  $0.05 \times d_{\text{obs}}$  for MAgent. Gumbel-softmax sparsification uses temperature  $\tau=0.5$  and adjacency threshold 0.6 throughout. For the group-conditional prior, we use  $g=2$  groups on 2-type maps and  $g=3$  on 3-type maps, with  $\sigma_{\text{intra}}=0.1$  and  $\sigma_{\text{cross}}=0.01$  (SMACv1/MAgent) or 0.05 (SMACv2). Group-prior warmup is 150k steps on SMACv1/MAgent and 100k on SMACv2. Each configuration is run with 5 random seeds. The IB regularizers add less than 5% wall-clock overhead.

## M Hyperparameter Sensitivity

This appendix section collects the hyperparameter-sensitivity evidence referenced from §5.4. We organize the knobs into two tiers.

---

**Algorithm 1** HIBCG Training (one gradient step)

---

**Require:** Observations  $\{o_i^t\}_{i=1}^n$ ; replay batch  $\mathcal{B}$ ; layer count  $L$ ; scalar capacity weights  $\lambda_{A,\text{dim}}, \lambda_{X,\text{dim}}$  (warmed up over  $T_{\text{warm}}$  steps); group-conditional prior scales  $\sigma_{0,\text{intra}}, \sigma_{0,\text{cross}}$ ; truncation horizon  $T_{\text{trunk}}$ ; noise scale  $\delta \in (0, 1]$

- 1: **Base GACG sample** (Eq. (1)): compute  $\boldsymbol{\mu}^t$  via attention; **if**  $t \geq T_{\text{trunk}}$ : compute group mask  $M^t$  from recent trajectory; set  $\Sigma_A^t = \alpha \widehat{\mathbf{M}}^t + \varepsilon I$ ; sample  $z_A^{(0)} \sim \mathcal{N}(\boldsymbol{\mu}^t, \Sigma_A^t)$ ; **else**: sample  $z_A^{(0)}$  via RelaxedBernoulli( $\boldsymbol{\mu}^t$ ); symmetrize and normalize to obtain  $A^{(0)}$
  - 2: Initialize  $Z_X^{(0)} \leftarrow \text{MLP}(X)$  {compressed per-agent input features}
  - 3: **for**  $l = 1$  **to**  $L$  **do**
  - 4:   **Structure encoder:**  $(\mu_A^{(l)}, \log \sigma_A^{2(l)}) \leftarrow f_A^{(l)}(A^{(0)}, Z_X^{(l-1)})$ ; sample  $\tilde{z}_A^{(l)} \leftarrow \mu_A^{(l)} + \delta \sigma_A^{(l)} \odot \varepsilon$ ,  $\varepsilon \sim \mathcal{N}(0, I)$
  - 5:   **Gate edges:** symmetrize and normalize  $\tilde{z}_A^{(l)}$ ;  $\tilde{A}^{(l)} \leftarrow g_l(\tilde{z}_A^{(l)})$  {e.g. sigmoid or hard threshold}
  - 6:   **Message passing:**  $Z_X^{(l)} \leftarrow \phi_l(\tilde{A}^{(l)} Z_X^{(l-1)} W_l)$
  - 7:   Accumulate  $\widehat{\text{AIB}}^{(l)}$  (Eq. (18)) using  $(\mu_A^{(l)}, \sigma_A^{2(l)})$  and group-conditional prior  $\sigma_0^2 = \sigma_{0,\text{intra}}^2$  (intra-group),  $\sigma_{0,\text{cross}}^2$  (inter-group)
  - 8: **end for**
  - 9: **Feature encoder (XIB):**  $(\mu_X, \sigma_X^2) \leftarrow (h_\mu(Z_X^{(L)}), \exp h_\sigma(Z_X^{(L)}))$ ;  $Z_X^{\text{out}} \leftarrow \mu_X + \sigma_X \odot \varepsilon$ ,  $\varepsilon \sim \mathcal{N}(0, I)$
  - 10: Compute  $\widehat{\text{XIB}}$  (Eq. (21)) using  $(\mu_X, \sigma_X^2)$
  - 11: **Agent input:** concatenate  $[X, \tanh(Z_X^{\text{out}})]$ ; forward through agent network to obtain  $Q$ -values
  - 12: **Value mixing:** compute  $Q_{\text{tot}}(s, \mathbf{u}; \theta)$  and target  $y$  (Eq. (22))
  - 13: **Form loss:**  $\mathcal{L} \leftarrow \mathcal{L}_{\text{TD}} + \lambda_g \mathcal{L}_g + \lambda_{A,\text{dim}} \cdot \sum_l \widehat{\text{AIB}}^{(l)} + \lambda_{X,\text{dim}} \cdot \widehat{\text{XIB}}$
  - 14: Backpropagate  $\nabla_\theta \mathcal{L}$ ; update  $\theta$ ; update target  $\theta^-$  (Polyak or periodic copy)
  - 15: **(Optional)** Dual ascent: update  $\lambda_{A,\text{dim}}, \lambda_{X,\text{dim}}$  (Section K)
- 

**Tier A (IB-specific): directly tied to the HIBCG theory.** These are the knobs that the propositions of §4.2 reason about; their sweeps also serve as ablations of the corresponding claim.

- **Prior shape**  $\sigma_{\text{intra}}/\sigma_{\text{cross}}$  (**Prop. 4.3**). Main-text Table 4 summarises the three-row sweep on 3s5z (wider, default, tight) and the reversed-prior stress test on MMM2. 3s5z WR varies by only 1.2 pp across the full sweep (ceiling effect on a 2-type map), while per-edge KLs swing by  $\sim 14\times$  (intra) and  $\sim 2.2\times$  (cross), confirming that the  $\sigma$  ratio is a clean dial for capacity allocation rather than for end performance. The MMM2 reversed-prior row is the key test: a positive HIBCG effect from the reversed prior would invalidate the “role-aligned asymmetry is doing the work” interpretation.
- **Message compression weight**  $\lambda_{X,\text{dim}}$  (**Prop. 4.5**). On 3s5z, the full sweep  $\lambda_X \in \{0.05, 0.1, 0.2, 0.3, 0.4, 0.5\}$  exhibits three regimes (main-body Prop. 4.5 paragraph): XIB-dominant at 0.5, XIB-collapsed at  $\leq 0.1$ , and balanced near 0.3. The balanced regime is the only one that simultaneously retains a non-trivial loss\_xib and reduces graph density below the AIB-only baseline, matching the water-filling prediction.
- **Group count**  $g$  (**Prop. 4.2**). Because Prop. 4.2 guarantees no regret for *any* block-diagonal prior containing the flat prior as a special case, HIBCG is expected to be no worse than HIB-flat for any choice of  $g$ , with the strongest gains when  $g$  matches the true role count  $m_{\text{true}}$ . We verify this with an off-by-one study on the heterogeneous maps (Table 12): on 1c3s5z ( $m_{\text{true}}=3$ ),  $g=2$  and  $g=3$  both match flat on WR while tightening the AIB loss; on MMM2 ( $m_{\text{true}}=3$ ),  $g=3$  is the clear winner, but even  $g=2$  remains competitive. This confirms that  $g$  behaves as a mild hyperparameter rather than a knife-edge choice, and aligns with our position that the group partition itself is GACG’s contribution (§2), not HIBCG’s.
- **Group-prior warmup**  $T_{\text{warm}}$ . On 3s5z (heterogeneous),  $T_{\text{warm}}=150\text{k}$  modestly improves WR\_final over no warmup (+1.3 pp), consistent with the idea that a stable groupniser helps the structural prior. On the homogeneous 8m\_vs.9m, the direction inverts (no-warmup +3.2 pp over warmup), because forcing a group prior into an essentially roleless setting hurts. Both results are consistent with Prop. 4.2: warmup amplifies a useful bias and amplifies a mis-specified one.

Table 12: Sensitivity to the group count  $g$  on heterogeneous maps (final WR,  $n \geq 4$  unless flagged). Performance is stable across  $g=m_{\text{true}} \pm 1$ , and HIBCG is no worse than HIB-flat in every cell—the no-regret guarantee of Prop. 4.2.

Map ( $m_{\text{true}}$ )	HIB-flat ( $g=1$ equiv.)	HIBCG $g=2$	HIBCG $g=3$
1c3s5z (3)	$0.910 \pm 0.038$	$0.905 \pm 0.024$	$0.912 \pm 0.010$
MMM2 (3)	$0.542 \pm 0.38$	$0.659 \pm 0.33$	<b><math>0.814 \pm 0.06</math></b>

**Tier B (inherited from GACG / EPyMARL): at most second-order in our ablations.** The adjacency threshold (GACG), Gumbel-softmax temperature, GCN message width  $r \cdot d_{\text{obs}}$ , and  $\lambda_{A,\text{dim}}$  follow values reported in GACG [10] and BVME [46]; their sweeps (documented in those papers and in our experiment logs) do not change any qualitative conclusion of §5. In particular: switching Gumbel temperature from 0.5 to 1.0 on 3s5z shifts final WR by  $< 1$  pp; raising the adjacency threshold from 0.5 to 0.6 reduces GD by  $\sim 2\times$  at comparable WR; and  $\lambda_{A,\text{dim}}$  enters the theory only through the water-filling multiplier (Prop. 4.5), so by construction it trades AIB rate for TD loss along the optimal curve rather than shifting the curve itself.

**Summary.** Across Tier-A knobs the direction of change always matches the prediction of the corresponding proposition (tighter priors  $\Rightarrow$  tighter KLS; higher  $\lambda_X \Rightarrow$  more message compression until the structural path is starved; higher  $g \Rightarrow$  finer capacity allocation but diminishing WR gains beyond  $m_{\text{true}}$ ). Tier-B knobs affect the GACG backbone but leave the HIBCG-over-backbone gap essentially unchanged. In the interest of space, full numerical tables for each Tier-A sweep are available in the appendix experiment log.

## References

- [1] S. Sukhbaatar, R. Fergus *et al.*, “Learning multiagent communication with backpropagation,” in *Advances in Neural Information Processing Systems (NeurIPS)*, vol. 29, 2016.
- [2] J. Jiang and Z. Lu, “Learning attentional communication for multi-agent cooperation,” in *Advances in Neural Information Processing Systems (NeurIPS)*, vol. 31, 2018.
- [3] A. Das, T. Gervet, J. Romoff, D. Batra, D. Parikh, M. Rabbat, and J. Pineau, “Tarmac: Targeted multi-agent communication,” in *International Conference on Machine Learning (ICML)*. PMLR, 2019, pp. 1538–1546.
- [4] C. Guo, H. Li, D. Qiu, H. Li, Y. Zhang, P. Li *et al.*, “A survey of multi-agent deep reinforcement learning with communication,” *Autonomous Agents and Multi-Agent Systems*, vol. 38, no. 1, p. 13, 2024.
- [5] J. Foerster, I. A. Assael, N. de Freitas, and S. Whiteson, “Learning to communicate with deep multi-agent reinforcement learning,” in *Advances in Neural Information Processing Systems (NeurIPS)*, vol. 29, 2016.
- [6] X. Liu and K. Bai, “Partially observable multi-agent rl with (quasi-)efficiency: The blessing of information sharing,” in *International Conference on Machine Learning (ICML)*. PMLR, 2023, pp. 22 106–22 130.
- [7] W. Duan, J. Lu, and J. Xuan, “Bayesian ego-graph inference for networked multi-agent reinforcement learning,” in *The Thirty-ninth Annual Conference on Neural Information Processing Systems (NIPS 2025)*, 2025.
- [8] T. Yang, J. Wang, L. Wu, and C. Zhang, “Context-aware sparse deep coordination graphs,” in *International Conference on Learning Representations (ICLR)*, 2022.
- [9] Q. Yang, W. Dong, Z. Ren, J. Wang, T. Wang, and C. Zhang, “Self-organized polynomial-time coordination graphs,” in *International Conference on Machine Learning (ICML)*, vol. 162, 2022, pp. 24 963–24 979.

- [10] W. Duan, J. Lu, and J. Xuan, “Group-aware coordination graph for multi-agent reinforcement learning,” in *Proceedings of the Thirty-Third International Joint Conference on Artificial Intelligence (IJCAI)*, 2024, pp. 3926–3934.
- [11] G. S. Varela, A. Sardinha, and F. S. Melo, “Networked agents in the dark: Team value learning under partial observability,” in *Proceedings of the 24th International Conference on Autonomous Agents and Multiagent Systems, AAMAS 2025, Detroit, MI, USA, May 19-23, 2025*. International Foundation for Autonomous Agents and Multiagent Systems / ACM, 2025, pp. 2087–2095.
- [12] S. Li, J. K. Gupta, P. Morales, R. E. Allen, and M. J. Kochenderfer, “Deep implicit coordination graphs for multi-agent reinforcement learning,” in *Proceedings of the 20th International Conference on Autonomous Agents and Multiagent Systems (AAMAS)*, 2021, pp. 764–772.
- [13] Y. Liu, W. Wang, Y. Hu, J. Hao, X. Chen, and Y. Gao, “Multi-agent game abstraction via graph attention neural network,” in *AAAI Conference on Artificial Intelligence*, 2020, pp. 7211–7218.
- [14] Y. Shi, S. Duan, C. Xu, R. Wang, F. Ye, and C. Yuen, “Dynamic deep factor graph for multi-agent reinforcement learning,” *IEEE Transactions on Pattern Analysis and Machine Intelligence*, vol. 48, no. 3, pp. 3417–3431, 2026.
- [15] T. N. Kipf and M. Welling, “Semi-supervised classification with graph convolutional networks,” in *5th International Conference on Learning Representations, ICLR 2017, Toulon, France, April 24-26, 2017, Conference Track Proceedings*. OpenReview.net, 2017.
- [16] W. Duan, J. Xuan, M. Qiao, and J. Lu, “Learning from the dark: Boosting graph convolutional neural networks with diverse negative samples,” in *Thirty-Sixth AAAI Conference on Artificial Intelligence (AAAI 2022), Virtual Event*. AAAI Press, 2022, pp. 6550–6558.
- [17] W. Duan, J. Lu, Y. G. Wang, and J. Xuan, “Layer-diverse negative sampling for graph neural networks,” *Transactions on Machine Learning Research*, 2024.
- [18] W. Duan, J. Xuan, M. Qiao, and J. Lu, “Graph convolutional neural networks with diverse negative samples via decomposed determinant point processes,” *IEEE Transactions on Neural Networks and Learning Systems*, vol. 35, no. 12, pp. 18 160–18 171, 2024.
- [19] Z. Yao, F. Huang, Y. Li, W. Duan, P. Qian, N. Yang, and W. Susilo, “Mecon: A gnn-based graph classification framework for MEV activity detection,” *Expert Syst. Appl.*, vol. 269, p. 126486, 2025.
- [20] J. Jiang, C. Dun, T. Huang, and Z. Lu, “Graph convolutional reinforcement learning,” in *International Conference on Learning Representations (ICLR)*, 2020.
- [21] T. Wang, R. Liao, J. Ba, and S. Fidler, “Nervenet: Learning structured policy with graph neural networks,” in *International Conference on Learning Representations (ICLR)*, 2018.
- [22] W. Böhmer, V. Kurin, and S. Whiteson, “Deep coordination graphs,” in *International Conference on Machine Learning (ICML)*, vol. 119. PMLR, 2020, pp. 980–991.
- [23] A. Das, T. Gervet, J. Romoff, D. Batra, D. Parikh, M. Rabbat, and J. Pineau, “Tarmac: Targeted multi-agent communication,” in *International Conference on Machine Learning (ICML)*. PMLR, 2019, pp. 1538–1546.
- [24] Y. Niu, R. R. Paleja, and M. C. Gombolay, “Multi-agent graph-attention communication and teaming,” in *Proceedings of the 20th International Conference on Autonomous Agents and Multiagent Systems (AAMAS)*, 2021, pp. 964–973.
- [25] W. Duan, J. Lu, and J. Xuan, “Inferring latent temporal sparse coordination graph for multiagent reinforcement learning,” *IEEE Transactions on Neural Networks and Learning Systems*, vol. 36, no. 8, pp. 14 358–14 370, 2025.

- [26] S. He, H. Ni, J. Wang, L. Wu, and C. Zhang, “Learning multi-agent communication from graph modeling perspective,” in *International Conference on Learning Representations (ICLR)*, 2024.
- [27] B. Lin and C. Lee, “HGAP: boosting permutation invariant and permutation equivariant in multi-agent reinforcement learning via graph attention network,” in *Forty-first International Conference on Machine Learning, (ICML 2024), Vienna, Austria, July 21-27, 2024*. OpenReview.net, 2024.
- [28] J. Weil, Z. Bao, O. Abboud, and T. Meuser, “Towards generalizability of multi-agent reinforcement learning in graphs with recurrent message passing,” in *Proceedings of the 23rd International Conference on Autonomous Agents and Multiagent Systems, (AAMAS 2024), Auckland, New Zealand, May 6-10, 2024*, 2024, pp. 1919–1927.
- [29] J. Yang, I. Borovikov, and H. Zha, “Hierarchical cooperative multi-agent reinforcement learning with skill discovery,” in *Proceedings of the 19th International Conference on Autonomous Agents and Multiagent Systems (AAMAS)*, 2020, pp. 1566–1574.
- [30] X. Li, X. Wang, C. Bai, and J. Zhang, “Exponential topology-enabled scalable communication in multi-agent reinforcement learning,” in *International Conference on Learning Representations (ICLR)*, 2025.
- [31] T. Wang, H. Dong, V. Lesser, and C. Zhang, “Roma: Multi-agent reinforcement learning with emergent roles,” in *International Conference on Machine Learning (ICML)*, 2020, pp. 9876–9886.
- [32] T. Phan, F. Ritz, L. Belzner, P. Altmann, T. Gabor, and C. Linnhoff-Popien, “VAST: Value function factorization with variable agent sub-teams,” in *Advances in Neural Information Processing Systems (NeurIPS)*, 2021, pp. 24 018–24 032.
- [33] S. Iqbal, C. A. S. de Witt, B. Peng, W. Böhmer, S. Whiteson, and F. Sha, “REFIL: Randomized extrapolation for multi-agent reinforcement learning,” in *International Conference on Machine Learning (ICML)*, 2021, pp. 4555–4566.
- [34] Y. Pan, J. Chen, B. Huang, D. Wang, and H. Deng, “Self-organized group for cooperative multi-agent reinforcement learning,” in *Advances in Neural Information Processing Systems (NeurIPS)*, 2022.
- [35] Z. Li, P. Liu, J. Chen, and C. Zhang, “Group-oriented multi-agent reinforcement learning,” in *International Conference on Machine Learning (ICML)*, 2023.
- [36] D. Kim, S. Moon, D. Hostallero, W. J. Kang, T. Lee, K. Son, and Y. Yi, “Learning to schedule communication in multi-agent reinforcement learning,” in *7th International Conference on Learning Representations, ICLR 2019*, 2019.
- [37] H. Mao, Z. Zhang, Z. Xiao, Z. Gong, and Y. Ni, “Learning agent communication under limited bandwidth by message pruning,” in *The Thirty-Fourth AAAI Conference on Artificial Intelligence, AAAI 2020, The Thirty-Second Innovative Applications of Artificial Intelligence Conference, IAAI 2020, The Tenth AAAI Symposium on Educational Advances in Artificial Intelligence, EAAI 2020, New York, NY, USA, February 7-12, 2020*. AAAI Press, 2020, pp. 5142–5149.
- [38] S. Dolan, S. Nayak, J. J. Aloor, and H. Balakrishnan, “Asynchronous cooperative multi-agent reinforcement learning with limited communication,” in *Proceedings of the 24th International Conference on Autonomous Agents and Multiagent Systems, (AAMAS 2025), Detroit, MI, USA, May 19-23, 2025*. International Foundation for Autonomous Agents and Multiagent Systems / ACM, 2025, pp. 2496–2498.
- [39] T. Wang, J. Wang, C. Zheng, and C. Zhang, “Learning nearly decomposable value functions via communication minimization,” in *International Conference on Learning Representations (ICLR)*, 2020.
- [40] T. Wang and C. Zhang, “Multi-agent shared information aggregation for cooperative multi-agent reinforcement learning,” in *International Conference on Machine Learning (ICML)*, 2023.
- [41] S. Ding, W. Du, L. Ding, J. Zhang, L. Guo, and B. An, “Robust multi-agent communication with graph information bottleneck optimization,” *IEEE Transactions on Pattern Analysis and Machine Intelligence*, vol. 46, no. 5, pp. 3096–3107, 2024.

- [42] N. Tishby, F. C. Pereira, and W. Bialek, “The information bottleneck method,” *Proceedings of the 37th Annual Allerton Conference on Communication, Control, and Computing*, pp. 368–377, 1999.
- [43] T. Wu, H. Ren, P. Li, and J. Leskovec, “Graph information bottleneck,” *Advances in Neural Information Processing Systems (NeurIPS)*, vol. 33, pp. 20 437–20 448, 2020.
- [44] A. A. Alemi, I. Fischer, J. V. Dillon, and K. Murphy, “Deep variational information bottleneck,” in *International Conference on Learning Representations (ICLR)*, 2017.
- [45] M. Igl, K. Ciosek, Y. Li, S. Tschiatschek, C. Zhang, S. Devlin, and K. Hofmann, “Generalization in reinforcement learning with selective noise injection and information bottleneck,” in *Advances in Neural Information Processing Systems 32: Annual Conference on Neural Information Processing Systems 2019, NeurIPS 2019, December 8-14, 2019, Vancouver, BC, Canada*, 2019, pp. 13 956–13 968.
- [46] W. Duan, J. Lu, and J. Xuan, “Bandwidth-constrained variational message encoding for multi-agent coordination,” in *Proceedings of the 25th International Conference on Autonomous Agents and Multiagent Systems (AAMAS)*, 2026.
- [47] Z. Liu, L. Wan, S. Sun, X. Sui, X. Chen, X. Lan, and N. Zheng, “Enhancing value decomposition with target transformation in cooperative multi-agent reinforcement learning,” *IEEE Transactions on Pattern Analysis and Machine Intelligence*, pp. 1–17, 2026.
- [48] T. Li and K. Zhu, “Efficient exploration for multi-agent diversity with agent identity,” *IEEE Transactions on Pattern Analysis and Machine Intelligence*, vol. 48, no. 5, pp. 5460–5473, 2026.
- [49] H. Hsu, W. Wang, M. Pajic, and P. Xu, “Randomized exploration in cooperative multi-agent reinforcement learning,” in *Advances in Neural Information Processing Systems 38: Annual Conference on Neural Information Processing Systems (NeurIPS 2024), Vancouver, BC, Canada, December 10 - 15, 2024*.
- [50] J. G. Kuba, R. Chen, M. Wen, Y. Wen, F. Sun, J. Wang, and Y. Yang, “Trust region policy optimisation in multi-agent reinforcement learning,” in *International Conference on Learning Representations (ICLR)*, 2022.
- [51] X. Yang, J. Lu, E. Yu, and W. Duan, “Resilient contrastive pre-training under non-stationary drift,” 2025. [Online]. Available: <https://arxiv.org/abs/2502.07620>
- [52] X. Yang, J. Lu, and E. Yu, “Walking the tightrope: Autonomous disentangling beneficial and detrimental drifts in non-stationary custom-tuning,” in *The Thirty-ninth Annual Conference on Neural Information Processing Systems*, 2025. [Online]. Available: <https://openreview.net/forum?id=1BAiQmAFsx>
- [53] —, “Adapting multi-modal large language model to concept drift from pre-training onwards,” in *The Thirteenth International Conference on Learning Representations*, 2025. [Online]. Available: <https://openreview.net/forum?id=b20VK2GnSs>
- [54] E. Yu, J. Lu, K. Wang, X. Yang, and G. Zhang, “Drift-aware collaborative assistance mixture of experts for heterogeneous multistream learning,” *arXiv preprint arXiv:2508.01598*, 2025.
- [55] F. A. Oliehoek and C. Amato, *A Concise Introduction to Decentralized POMDPs*, ser. Springer Briefs in Intelligent Systems. Springer, 2016.
- [56] T. Rashid, M. Samvelyan, C. S. de Witt, G. Farquhar, J. N. Foerster, and S. Whiteson, “QMIX: monotonic value function factorisation for deep multi-agent reinforcement learning,” in *Proceedings of the 35th International Conference on Machine Learning (ICML 2018), Stockholmsmässan, Stockholm, Sweden*, vol. 80, 2018, pp. 4292–4301.
- [57] T. M. Cover and J. A. Thomas, *Elements of Information Theory*, 2nd ed. Wiley-Interscience, 2006.

- [58] M. Samvelyan, T. Rashid, C. Schröder de Witt, G. Farquhar, N. Nardelli, T. G. J. Rudner, C.-M. Hung, P. H. S. Torr, J. Foerster, and S. Whiteson, “The starcraft multi-agent challenge,” in *Proceedings of the 18th International Conference on Autonomous Agents and MultiAgent Systems (AAMAS)*, 2019, pp. 2186–2188.
- [59] B. Ellis, J. Cook, S. Moalla, M. Samvelyan, M. Sun, A. Mahajan, J. N. Foerster, and S. Whiteson, “Smacv2: An improved benchmark for cooperative multi-agent reinforcement learning,” in *The 36th Annual Conference on Neural Information Processing Systems (NeurIPS 2023), New Orleans, LA, USA, December 10 - 16, 2023*.
- [60] L. Zheng, J. Yang, H. Cai, M. Zhou, W. Zhang, J. Wang, and Y. Yu, “Magent: A many-agent reinforcement learning platform for artificial collective intelligence,” in *AAAI Conference on Artificial Intelligence*, 2018, pp. 8222–8223.